

GemPy 1.0: open-source stochastic geological modeling and inversion

Miguel de la Varga, Alexander Schaaf, and Florian Wellmann

Institute for Computational Geoscience and Reservoir Engineering

Correspondence to: varga@ices.rwth-aachen.de

Abstract. The representation of subsurface structures is an essential aspect of a wide variety of geoscientific investigations and applications: ranging from geofluid reservoir studies, over raw material investigations, to geosequestration, as well as many branches of geoscientific research studies and applications in geological surveys. A wide range of methods exists to generate geological models. However, especially the powerful methods are behind a paywall in expensive commercial packages. We present here a full open-source geomodeling method, based on an implicit potential-field interpolation approach. The interpolation algorithm is comparable to implementations in commercial packages and capable of constructing complex full 3-D geological models, including fault networks, fault-surface interactions, unconformities, and dome structures. This algorithm is implemented in the programming language Python, making use of a highly efficient underlying library for efficient code generation (theano) that enables a direct execution on GPU's. The functionality can be separated into the core aspects required to generate 3-D geological models and additional assets for advanced scientific investigations. These assets provide the full power behind our approach, as they enable the link to Machine Learning and Bayesian inference frameworks and thus a path to stochastic geological modeling and inversions. In addition, we provide methods to analyse model topology and to compute gravity fields on the basis of the geological models and assigned density values. In summary, we provide a basis for open scientific research using geological models, with the aim to foster reproducible research in the field of geomodeling.

Contents

20	1 Introduction	16
	2 CORE – Geological modeling with GemPy	18
	2.1 Geological modeling and the potential-field approach	18
	2.1.1 Concept of the potential-field method	18
	2.1.2 Adjustments to structural geological modeling	20
25	2.2 Geological model interpolation using <i>GemPy</i>	22
	2.2.1 From scalar field to geological block model	22

	2.2.2	Combining scalar fields: Depositional series and faults	24
	2.3	"Under the hood": The <i>GemPy</i> architecture	27
	2.3.1	The graph structure	27
30	2.3.2	Theano	29
	3	ASSETS – Model analysis and further use	31
	3.1	Visualization	32
	3.2	Gravity forward modeling	33
	3.3	Topology	35
35	3.4	Stochastic Geomodeling and probabilistic programming	37
	3.4.1	Uncertainty Quantification	39
	3.4.2	Geological inversion: Gravity and Topology	42
	4	Discussion	46
		Appendix A: GemPy package information	50
40		Appendix A1: Installation	50
		Appendix A2: Documentation	51
		Appendix A3: Jupyter notebooks	51
		Appendix A4: Unit Tests	51
		Appendix B: Kriging system expansion	51
45		Appendix B1: Gradient Covariance-Matrix $C_{\partial \mathbf{z} / \partial \mathbf{u}}$	51
		Appendix B2: Interface Covariance-Matrix	54
		Appendix B3: Cross-Covariance	55
		Appendix B4: Universal matrix	56
		Appendix C: Kriging Estimator	56
50		Appendix D: Example of covariance function: cubic	57
		Appendix E: Probabilistic Graphical Model <u>checking and diagnostics</u>	58
		Appendix F: Blender integration	60

Answer Review 1:

Thank you very much for your suggestions, detailed comments and questions, as well as the positive feedback. We carefully revised the manuscript and provide below a detailed reply to all comments. We also attached a pdf with highlighted changes between the original submission and the revised version.

We agree with the reviewer that the explanation of the Bayesian network was not clear and probably insufficient. However, the scope of this particular paper was on the generative model of the Bayesian inference. Since the whole library has been written to be part of a Bayesian inference, we consider it appropriate to just to show a vertical slice of what is possible. Nevertheless, we have reworked quite that part of the paper quite a bit and now include the whole probabilistic graphical model into the main text in order to be more consistent and clear. Also, we have added the convergence analysis in the appendix.

Regarding the reviewers general concerns about the construction of the likelihood functions and samplers, we shared many of them and we are working hard to find the optimal Bayesian model for different data sets. The comments were very insightful and hopefully we will be able to explore them in a more focused paper in the future.

RESPONSES

[1] The paper would benefit from a clear and concise description of an example of at least one probabilistic model.

Authors response: We have extended and moved to the main text the specific probabilistic graphical model

Change in manuscript:

[1a] For example in section 3.4.2 Geological Inversion: Gravity and Topology the authors say that they construct a specific likelihood function for a topolC2 GMDD Interactive comment Printer-friendly version Discussion paper ogy, but no likelihood function is given. The authors correctly state that the Jaccard index varies between 0 and 1, but then go on to state that it is a single number we can evaluate using a a probability density function. The type of probability density function used will determine the strength or likelihood that the mean graph represent. What does this sentence mean? They go on to say Here we use a half Cauchy, due to tolerance for outliers. Why? A half Cauchy has support on the interval $[0, \infty)$, whereas this statistic has support on the interval $[0, 1]$. What is meant by its tolerance for outliers?

Authors response: We use a half-Cauchy distribution to evaluate the likelihood of the Jaccard index of the simulated model topology due to its wider tail. It is not used directly as a likelihood, but rather as a factor potential which allows us to incorporate the “soft data” of our topology information into the Bayesian inference. As the Jaccard index results in values within the interval $[0,1]$, the half-Cauchy function is only evaluated for those given values. The shape parameter β was chosen empirically, as it showed promising results for effective parameter space exploration in the used MCMC

scheme.

Change in manuscript: *To evaluate the likelihood of the simulated model topology we use a factor potential with a half-Cauchy parametrization (shape parameter $\alpha=0$ and rate parameter $\beta=10^{-3}$) to constrain our model using the “soft data” of our topological knowledge \cite{lauritzen1990independence,jordan1998learning,christakos2002assimilation}. This specific parametrization was chosen due to empirical evidence from different model runs to allow for effective parameter space exploration in the used MCMC scheme.*

[1b] What is needed is a joint likelihood function on both the topology and the gravity to be specifically stated. See for example () and (). The authors should at least reference ().

Authors response: In pymc when you specify more than one likelihood/potential, it automatically starts sampling on the joint likelihood.

Change in manuscript: [1010] *Defining the topology potential and gravity likelihood on the same Bayesian network creates a joint likelihood value that we need to sample from*

[1c] The authors statement The use of likelihood functions in a Bayesian inference in opposition to simply rejection sampling has been explored by the authors during the recent years (de la Varga and Wellmann, 2016; Wellmann et al., 2017; Schaaf, 2017). is confusing. Are the authors referring to likelihood free methods such as Approximate Bayesian Computation, ABC, where rejection sampling can be used to obtain draws from the approximate posterior? The use of likelihood function in Bayesian inference is typically not related to rejection sampling. Rejection sampling is a method to obtain draws from a non-standard distribution, in this case the posterior distribution, usually for the purpose of numerical integration. A likelihood is an assumption about the data generation process which, together with the prior, result in inference via the posterior. If the likelihood is unavailable in closed form, or if we do not wish to make assumptions about the data generating process, then the issue of how to approximate the posterior may involve rejection sampling. The authors need to articulate clearly the point they are making and provide a justification.

Authors response: In the sentence we were confusing rejection sampling as a parameter space exploration method to approximate a posterior with just forward simulating the priors. We agree with the reviewers comments and adjusted the sentence in line 855.

Change in manuscript [855]: *“The use of likelihood functions in a Bayesian inference in comparison to simple forward simulation has been explored by the authors during recent years (de la Varga and Wellmann, 2016; Wellmann et al., 2017; Schaaf, 2017).”*

[1d] A gravity likelihood is referred to on page 31. What is this likelihood? Are the authors assuming that the observed data is related to the simulated data as a signal plus noise model of the form, $y_i = g(x_i) + e_i$, where e_i is independently and identically distributed (i.i.d)? If so why do they model $(y_i - g(x_i))^2$ as a folded Cauchy (i.e a folded t_1)? What is this saying about the data generating process? Surely there is geophysical

knowledge about the distribution of gravity measurements? From a statistical point of view gravity is an integral, a sum of things, in which case the central limit theorem (CLT) would make the assumption of Gaussian errors, i.e. $\epsilon_i \sim N(0, \sigma^2)$, reasonable. If this were so then and the observations independent (which I'm not convinced they would be), then $\sum_{i=1}^n (y_i - g(x_i))^2 \sim \chi^2_{2n}$. Perhaps this is what they do, but it is not clear from the paper

Authors response: We agree with the reviewer that the explanation was not sufficiently clear, in part because it was not the main purpose of this paper and in part because we did not find yet a convincing way to construct the likelihood function. The model suggested by the reviewer is quite close to what we presented here and we agree with his concerns about the correlation but again we prefer to focus around the generative model since the paper is already too large. Nevertheless, we have extended the explanation of this part and adding the complete PGM figure into the main body text

[2] MCMC convergence The authors need to show that the MCMC scheme converges. Convergence in geophysical inversion problems is non trivial. Posterior distributions of geophysical inversion problems are notoriously difficult to explore, for a discussion see (). and for a demonstration of how difficult they are to explore see (). The NUTS algorithm used in python works well when the derivative exists and is well behaved, but as the posterior distribution in () shows, these distributions can have many modes and derivatives which are difficult, if not impossible to compute. Parallel tempering is probably the best way to explore these multi-model distributions, as shown in ().

Authors response: We added a traces plot and a Geweke test into the appendix. Again, we share the concerns about the samplers and we are actively studying the best combinations of them for this type of problems. We agree that a combination of gradient based and parallel methods could be the best solution in the middle term. However, we also consider that that is beyond the scope of this publication.

[3a] The Jaccard index given by equation 13 is not a likelihood function, nor, as it is written, is it even a measure. The authors correctly state that the Jaccard index is a statistic used to compare sets, in this case topologies. It is the ratio of the size of the intersection over size of the union. It should be written as

$$J(A, B) = |A \cap B| / |A \cup B|$$

where the notation $|\cdot|$ denotes a measure of size to be defined.

Authors response: Adjusted Jaccard index to correctly contain the absolutes. Thanks for catching this!

Change in manuscript: Changed Eq. 13 to $J(A, B) = |A \cap B| / |A \cup B|$

[3b] change the phrase due to tolerance for outliers to because parameter estimates based on Cauchy likelihoods are more robust to outliers than param-

eter estimates based on, say, Gaussian likelihoods.

Authors response: We agree to the change in wording, but adjusted the whole paragraph to more precisely state the use of the topology information as a factor potential in the Bayesian inference and the second reviewers comments on line [811].

Change in manuscript: *To evaluate the likelihood of the simulated model topology we use a factor potential with a half-Cauchy parametrization (shape parameter $\alpha=0$ and rate parameter $\beta=10^{-3}$) to constrain our model using the “soft data” of our topological knowledge \citep{lauritzen1990independence, jordan1998learning, christakos2002assimilation}. This specific parametrization was chosen due to empirical evidence from different model runs to allow for effective parameter space exploration in the used MCMC scheme and due to the Cauchy distribution being more robust to outliers than parameter estimates based on, say, Gaussian likelihoods.*

Answer Review 2:

Thank you very much for the detailed suggestions and comments and questions, as well as the positive feedback. After incorporating your input, the paper has become much more polished and easier to understand.

Despite agreeing with most of the recommendations about expanding the explanations about the probabilistic graphical models and fault networks, we are the opinion that the extent of the paper is already too large to incorporate this information. Therefore sections that may be self contained in further publications—i.e. Bayesian network, fault network—or that have been already published (although sadly quite sparsely) have been reworked but not extended. Hopefully all of this will come together in the firsts author PhD thesis.

Regarding the Bayesian model, the scope of this particular paper was on the generative model of the Bayesian inference—i.e. the mathematical formulation that connects the model parameters with different datasets. We have improved the clarity of our description and added the probabilistic graphical model into the main text.

The definition of faults drift functions are, again, too broad to be treated in an already too large paper. So far the drift function is manually defined and in the authors view the best results would be yielded by optimization. We are not aware of work done in this direction and we have just started to explore this option. Regarding their definition in the GemPy code, we have added some further explanation in the manuscript but, in short, it is done by categorizing the input data. Although in the paper we aim to give a flavour of the use of GemPy, for a good understanding of how to create models, we recommend the online documentation and tutorials (an endless work-in-progress). We will try to provide an example of fault networks sooner rather than later.

Finally, we took the decision of writing this paper as a compendium of the necessary algebra with the correspondent open-source code to generate implicit geological models. We are aware that a more extensive explanation of the kriging system and the Appendix C would be useful for the community but our mathematical knowledge is limited and we are not convinced of being able to add much value to the already published work in this

matter. Therefore we have opted for a more descriptive approach referencing the original sources.

Once again, we highly appreciate all comments and we accepted most suggestion not only for this paper but also for future work.

RESPONSES

Answer to pdf comments:

[73] reword

Authors response: reworded.

Change in manuscript: *The method was first introduce by \ cite{ Lajaunie.1997} and it is grounded on the mathematical principles of Universal CoKriging.*

[102] I would also say to provide an environment/ecosystem to improve/enhance/add existing methodologies.

Authors response: Accepted suggestion

Change in manuscript: *... , but to provide an environment to enhance existing methodologies as well as give access to an advanced modeling algorithm for scientific experiments in the field of geomodeling.*

[135] I wouldn't refer to this as anisotropy. More precisely, it describes the planar orientation of the stratigraphic structure throughout the volume.

Authors response: Accepted suggestion. We agree, it is less confusing now

Change in manuscript: *The gradient of the scalar field will follow the planar orientation of the stratigraphic structure throughout the volume or, in other words...*

[143] reword

Authors response: Reword:

Change in manuscript: *...as it is not possible to obtain remotely accurate estimations*

[168] why 0 subscript? shouldn't the function 's variable be a general point x?

Authors response: Further explanation and added citation. x_0 is the terminology used by Chiles on his book Geostatistics Modeling Spatial Uncertainty and the sub index 0 is used to differentiate the interpolated points x_0 to the input data x_α .

Change in manuscript: *where $\{ \backslash bf{ x} \} _{ 0}$ \$ refers to the estimated quantity*

for some integrable measure p_0 we will try to be especially verbose regarding the mathematical terminology based primarily on \cite{Chiles.2004}

[173] ?; unclear (and can lead to confusion) and not needed.

Authors response: Reword but not deleted. Despite we agree with the reviewer that the parameter p may lead to confusion we have decided to keep the original sentence for two reason:

- 1) Keep the nomenclature consistent with Chiles description
- 2) To point out that the method is multivariate and there is no limitations to extend the current mathematical formulation

[184] keep the terminology consistent, change to scalar field

Authors response: Potential field naming fixed, p substituted by ρ and u defined as any unit vector. Everything here was carelessness from our side. Thank you to the reviewer for pointing them out.

[188] unclear

Authors response: Reword.

Change in manuscript: *Note that in this context the scalar field property α is dimensionless. The only limitation is that the value must increase in the direction of the gradient which in turn describes the stratigraphic deposition.*

[195] Mention here that the choice of the reference point does not matter - choosing different reference points has no effect on the results.

Authors response: Added suggestion about reference point.

Change in manuscript: *It is important to mention that the choice of the reference points $\{\alpha_x\}_{\alpha=0}^k$ has no effect on the results.*

[200] most of this is unclear

Authors response: Improved explanation

Change in manuscript: *The advantage of this mathematical construction is that by not fixing the values of each interface $\{Z\}(\{x\}_{\alpha=0}^k)$, the compression of layers—i.e. the rate of change of the scalar field—will be only defined by the gradients $\{\partial Z\}(\partial u)$. This allows to propagate the effect of each gradient beyond the surrounding interfaces creating smoother formations.*

[209] define after this equation.

Authors response: Extended eq 3 definition

[210] Although this system is indeed correct. I am concerned that for most readers this system will be confusing. I would strongly suggest that appendix section C2 be expanded to explain in detail the meaning of this system and its clear consequences. Then from that derive separate linear systems for both the scalar field and the gradient of the scalar field. In addition, refer in lines 210-215 to that appendix section for full details.

Authors response: After long consideration. We have decided to leave it as system for two reason: (i) a proper explanation of a CoKriging system would need to be too long and we may not have the mathematical background to explain error-free, and (ii) the matricial form is more consistent—at least to us—with Chiles book explanation.

[217] on the right you have a 3x2 matrix

Authors response: Fixed terminology

[220] this description is insufficient. e.g. $f10 = f1(x0)$ and you never defined what $x0$ is. same goes for $f20$. In connection with my comment about eqn 4 you should show or say why $f10$ reduces to zero in the appendix. It would tremendously help new researchers fully understand the mathematics for potential enhancements - just as you have done for most of the kriging system.

Authors response: Added suggestions

[300] How do you ensure that the modelled conformable stratigraphic layers respect the specified sequence for the stratigraphic pile? e.g. the interpolation constraints for interface pts (the increment points) is that the scalar field at these interface pts is the same - the is no method of inputting the sequence via the increments since their particular value has no effect. This problem usually only presents itself when interface data is characterize by strong horizontally sampling bias.

Authors response: Added explanation. If we are not mistaken the reviewer refers here to the order of the formations within each series. Indeed this only depends on the geometry and now we added a sentence clarifying this point

Change in manuscript: *It is interesting to point out that the the sequential pile only controls the order of each individual series. Within each series, the stratigraphic sequence is strictly determined by the geometry and the interpolation algorithm.*

[345] why is there no input data for the fault and the unconformity?

Added explanation. The separation between the different series/faults is done by labeling the input data. As the paper only contains a small snippet of the code this was indeed misleading. We increased the comments on the listing hoping to clarify this point.

[370] spelling

Authors response: Corrected

[376] which rules?

Reworded. We are aware that the fault section is a bit too vague but again the paper is already too long and the faulting algorithms may fit in future work.

[379] how does one choose the perfect drift function? trial and error?

Authors response: Essentially yes, i.e. optimization. Nobody so far has come out with a better idea. Probably our framework would be the ideal place to test some of this since with AD optimizations work better.

[391-392] ?; unclear explicitly state what you mean by input parameters

Authors response: Reworded

Change in manuscript: *variables*

[401] explicitly define graph in the current context

Authors response: Reworded and added explanation of symbolic graph

Change in manuscript: *Writing symbolically requires a priori declaration of all algebra, from variables which will behave as latent parameters—i.e. the parameters we try to tune for optimization or uncertainty quantification—to all involved constants and the specific mathematical functions that relates them. This statements generate a so called graph that encapsulates symbolically all the logic what enables to perform further analysis on the logic itself (e.g. differentiation or optimization).*

[455] colloquial. please reword. can a method have intuitions?

Authors response: Reworded

Change in manuscript: *There is extensive literature explaining in detail the method and its related intuitions since it*

[498] these have not yet been defined yet - as it relates to implicit modelling

Authors response: Added reference to chapter

[FIGURE 6] Very confusing figure

Authors response: Reworked in 3D to improve clarity

[575] what is this variable?

Authors response: Added explanation

Change in manuscript: $t_{\mathcal{S}}$ —i.e. the distance dependent side of Equation \ref{eq:grav_0} —

[643] how is this done?

Authors response: Added explanation to paragraph

Change in manuscript: We multiply the binary fault array (0 for foot wall, 1 for hanging wall) with the maximum lithology value incremented by one. We then add it to the lithology array to make sure that layers that are in contact across faults are assigned a unique integer in the resulting array.

[720] Is there a best practices guide for PGM construction?

Authors response: Added some references. Sadly making Bayesian models nowadays is pretty much an art. The variability on topics datasets and complexity makes very difficult to give a close set of rules to construct the models. Probably the best reference would be Bayesian methods for hackers but seems to generalistic for the paper scope. Our past work and but in especial our future work will try to address this problem in a comprehensive manner since we agree that there is a lack guidelines especially in geological modeling

Relevant citations with bibkeys:

- {bishop2013model} Bishop, C. M. (2013). *Model-based machine learning*. *Phil. Trans. R. Soc. A*, 371(1984), 20120222.
- {sucar2015probabilistic} Sucar, L. E. (2015). *Probabilistic Graphical Models. Advances in Computer Vision and Pattern Recognition*. London: Springer London. doi, 10, 978-1.
- {Patil:FseZoIYV} Patil, A., Huard, D., & Fonnesbeck, C. J. (2010). *PyMC: Bayesian stochastic modelling in Python*. *Journal of statistical software*, 35(4), 1.
- {Koller:2009wk} Koller, D., & Friedman, N. (2009). *Probabilistic graphical models: principles and techniques*. MIT press.

[734] Why just the Z axis? It should be perturbed along each of the 3 axis. Does just choosing the one axis easier for generating results?

Authors response: Added explanation

The choice of perturbing only the Z axis is merely due to computational limitations. Uncertainty tends to be higher in this direction (e.g. wells data or seismic velocity), however there is a lot of room for further research on the definition of prior data—i.e. its choice and probabilistic description—on both directions, to ensure that we properly explore the space of feasible models and to generate a parametric space as close as possible to the posterior.

[744] reword

Authors response: Reworded

[765] what is the meaning of this variable?

Authors response: Removed . This is a pymc 2 dummy value to initialize the object. I just deleted it to avoid confusion.

[FIGURE 8 CAPTION] is this the number of realizations?; says probability of layer 2 in the figure! not layer 1

Authors response: Increased verbosity, fixed typo

[850] should change to p_i represents the probability of a layer at the i -th cell.

Authors response: Fixed typo

[851] compress? you mean quantity?

Authors response: Reworded

Change in manuscript: *we can use information entropy to reduce the dimensionality of probability fields into a single value at each voxel as an indication of uncertainty,*

[856] ? comparison

Authors response: Reworded

[881] what are these parameters? you also used alpha and beta elsewhere for something else

Authors response: Change in manuscript to specify parameters and how the topology is evaluated in the PGM:

Change in manuscript: *To evaluate the likelihood of the simulated model topology we use a factor potential with a half-Cauchy parametrization (shape parameter $\alpha=0$ and rate parameter $\beta=10^{-3}$) to constrain our model using the “soft data” of our topological knowledge \citep{lauritzen1990independence, jordan1998learning, christakos2002assimilation} . This specific parametrization was chosen due to empirical evidence from different model runs to allow for effective parameter space exploration in the used MCMC scheme and due to the Cauchy distribution being more robust to outliers than parameter estimates based on, say, Gaussian likelihoods.*

[948] reword

Authors response: Reworded

To sample from the posterior we use adaptive Metropolis

[958-961] reword; Also which example ? from Fig 8's posterior models?

Authors response: Specified figure and reworded explanation

[1018] spelling

Authors response: Fixed

[1036] reword

Authors response: Fixed

Change in manuscript: *up to now*

[1037] reword

Authors response: Fixed

Change in manuscript: *able to construct*

[1067] general?

Authors response: Fixed

Change in manuscript: *general*

[FIGURE 9] Why are you presenting this graph? It does not add any insight. Please remove

Authors response: Reworked figures and equations. The reason to add this figures was to clarify the different distances that goes to each covariance functions since for us were one of the main challenges. However we agree that the implementation was not very clear. Hopefully after the rework the use of the figures is more obvious

[1159] please define h_x , h_y . shouldn't this be $r = \sqrt{(h_x^2 + h_y^2 + h_z^2)}$ with $h_x = x_i - x_j$, $h_y = y_i - y_j$, $h_z = z_i - z_j$

Authors response: Added suggestion and reworded.

Change in manuscript:

$\backslash \begin{equation}$

$r = \sqrt{h_x^2 + h_y^2 + h_z^2}$

$\backslash \end{equation}$

and h_u as the distance $u_i - u_j$ in the given direction (usually Cartesian directions). Therefore, since we aim to derive $C_{\{Z\}}(r)$ respect an arbitrary direction u we must apply the $\backslash \textit{directional derivative}$ rules as follows:

[1164] repeat wrt lhs

Authors response: Fixed

[1175] reword; its related to the smoothness of a function

Authors response: Reworded and further explanation

Change in manuscript: *This derivation is independent to the covariance function of choice. However, some covariances may lead to mathematical indeterminations if they are not sufficiently differentiable.*

[FIGURE 10] Why are you presenting this graph? It does not add any insight. what do the different colored dots, lines, and arrows represent?

Authors response: same as Figure 9

[1186] keep terminology consistent throughout manuscript. change to scalar

Fixed

[FIGURE 11] Again, its unclear what the purpose of these graphs are trying to convey.

Authors response: same as figure 9

[1194] this eqn is incorrect. you have to be very careful with the notation. to properly show this you will have to restructure this.

Authors response: Fixed. Thank you for realizing. This was an important mistake.

[1195] ???

Authors response: Reworded.

Change in manuscript: *As the interfaces are relative to a reference point per later $\{ \backslash bf{ x} \} _{ - \{ \backslash alpha _{ - \backslash , 0} \} ^ k}$ the value of the covariance function will be the difference between this point and the rest on the same layer:*

[1196] formatting problem

Authors response: Fixed formatting

[1214] formatting errors. ; fii should be beta I assume

Authors response: Fixed formatting

[1220] Is there another reference for this? Matheron, 1981 is cryptic and written in a time (type writers) where there are no matrices in their explicit form. This reference is what is given in Lajaunie, but if there is a better reference can you add that?

Authors response: Added Chiles and Delfiner 2009 book reference

[1235] ??; these functions also have limits - especially so in scenarios where data sample highly variant geological structures.

[1238] before you indicated that C_0 is the value for the nugget effect.

Authors response: Fixed

[1245-46] grammar; not clear how one inputs the nugget effect given D1

Authors response: Added short explanation about nugget effect.

Change in manuscript: *The implementation of nugget effects in covariance matrices are done by adding the value to the diagonal.*

[FIGURE 13] Explain in more depth this figure. what are the "modifiers", why are there 11 of them?

Authors response: Whole PGM has been reworked manually and added to the main text.

1 Introduction

We commonly capture our knowledge about relevant geological features in the subsurface in the form of geological models, as 3-D representations of the geometric structural setting. Computer-aided geological modeling methods have existed for decades, and many advanced and elaborate commercial packages exist to generate these models (e.g. GoCAD, Petrel, GeoModeller). But even though these packages partly enable an external access to the modeling functionality through implemented API's or scripting interfaces, it is a significant disadvantage that the source code is not accessible, and therefore the true inner workings are not clear. More importantly still, the possibility to extend these methods is limited—and, especially in the current rapid development of highly efficient open-source libraries for machine learning and computational inference (e.g. *TensorFlow*, *Stan*, *pymc*, *PyTorch*, *Infer.NET*), the integration into other computational frameworks is limited.

Yet, there is to date no fully flexible open-source project which integrates state-of-the-art geological modeling methods. Conventional 3-D construction tools (CAD, e.g. *pythonOCC*, *PyGem*) are only useful to a limited extent, as they do not consider the specific aspects of subsurface structures and the inherent sparsity of data. Open source GIS tools exist (e.g. QGIS, *gdal*), but they are typically limited to 2-D (or 2.5-D) structures and do not facilitate the modeling and representation of fault networks, complex structures like overturned folds or dome structures), or combined stratigraphic sequences.

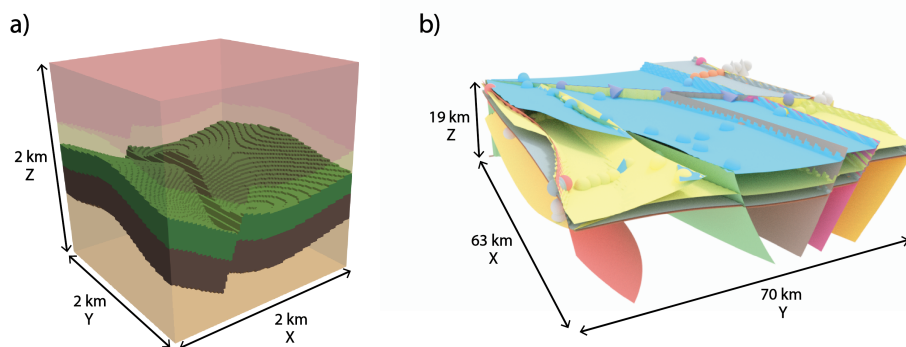


Figure 1. Example of models generated using *GemPy*. a) Synthetic model representing a reservoir trap, visualized in Paraview (Stamm, 2017); b) Geological model of the Perth basin (Australia) rendered using *GemPy* on the in-built Python in Blender (see appendix F for more details), spheres and cones represent the input data.

With the aim to close this gap, we present here *GemPy*, an open-source implementation of a modern and powerful implicit geological modeling method based on a potential-field approach; found, in turn, on a Universal CoKriging interpolation (Lajaunie et al., 1997; Calcagno et al., 2008). The method was first introduced by Lajaunie et al. (1997) and it is grounded on the mathematical principles of Universal CoKriging. In distinction to surface-based modeling approaches (see Caumon et al., 2009, for a good overview), these approaches allow the direct interpolation of multiple

conformal sequences in a single scalar field, and the consideration of discontinuities (e.g. metamorphic contacts, unconformities) through the interaction of multiple sequences (Lajaunie et al., 1997; Mallet, 2004; Calcagno et al., 2008; Caumon, 2010; Hillier et al., 2014). Also, these methods allow the construction of complex fault networks and enable, in addition, a direct global interpolation of all available geological data in a single step. This last aspect is relevant, as it facilitates the integration of these methods into diverse other workflows. Most importantly, we show here how we can integrate the method into novel and advanced machine learning and Bayesian inference frameworks (Salvatier et al., 2016) for stochastic geomodeling and Bayesian inversion. Recent developments in this field have seen a surge in new methods and frameworks, for example using gradient-based Monte Carlo methods (Duane et al., 1987; Hoffman and Gelman, 2014) or variational inferences (Kucukelbir et al., 2016), making use of efficient implementations of automatic differentiation (Rall, 1981) in novel machine learning frameworks. For this reason, *GemPy* is built on top of *Theano*, which provides not only the mentioned capacity to compute gradients efficiently, but also provides optimized compiled code (for more details see Section 2.3.2). In addition, we utilize *pandas* for data storage and manipulation (McKinney, 2011), Visualization Toolkit (*vtk*) Python-bindings for interactive 3-D visualization (Schroeder et al., 2004), the de facto standard 2-D visualization library *Matplotlib* (Hunter, 2007) and *NumPy* for efficient numerical computations (Walt et al., 2011). Our implementation is specifically intended for combination with other packages, to harvest efficient implementations in the best possible way.

Especially in this current time of rapid developments of open-source scientific software packages and powerful machine learning frameworks, we consider an open-source implementation of a geological modeling tool as essential. We therefore aim to open up this possibility to a wide community, by combining state-of-the-art implicit geological modeling techniques with additional sophisticated Python packages for scientific programming and data analysis in an open-source ecosystem. The aim is explicitly not to rival the existing commercial packages with well-designed graphical user interfaces, underlying databases, and highly advanced workflows for specific tasks in subsurface engineering, but to provide [an environment to enhance existing methodologies as well as give](#) access to an advanced modeling algorithm for scientific experiments in the field of geomodeling.

In the following, we will present the implementation of our code in the form of core modules, related to the task of geological modeling itself, and additional assets, which provide the link to external libraries, for example to facilitate stochastic geomodeling and the inversion of structural data. Each part is supported/ supplemented with Jupyter Notebooks that are available as additional online material and part of the package documentation, which enable the direct testing of our methods (see Section A3). These notebooks can also be executed directly in an online environment (Binder). We encourage the reader to use these tutorial Jupyter Notebooks to follow along the steps explained in the following. We encourage the reader to use these tutorial Jupyter Notebooks to follow along the steps explained in the following. Finally, we discuss our approach, specifically also with respect to

alternative modeling approaches in the field, and provide an outlook to our planned future work for this project.

2 CORE – Geological modeling with GemPy

130 In this section, we describe the core functionality of *GemPy*: the construction of 3-D geological models from geological input data (surface contact points and orientation measurements) and defined topological relationships (stratigraphic sequences and fault networks). We begin with a brief review of the theory underlying the implemented interpolation algorithm. We then describe the translation of this algorithm and the subsequent model generation and visualisation using the Python front-end
135 of *GemPy* and how an entire model can be constructed by calling only a few functions. Across the text, we include code snippets with minimal working examples to demonstrate the use of the library.

After describing the simple functionality required to construct models, we go deeper into the underlying architecture of *GemPy*. This part is not only relevant for advanced users and potential developers, but also highlights a key aspect: the link to *Theano* (Theano Development Team, 2016),
140 a highly evolved Python library for efficient vector algebra and machine learning, which is an essential aspect required for making use of the more advanced aspects of stochastic geomodeling and Bayesian inversion, which will also be explained in the subsequent sections.

2.1 Geological modeling and the potential-field approach

2.1.1 Concept of the potential-field method

145 The potential-field method developed by Lajaunie et al. (1997) is the central method to generate the 3D geological models in *GemPy*, which has already been successfully deployed in the modeling software GeoModeller 3-D (see Calcagno et al., 2008). The general idea is to construct an interpolation function $\mathbf{Z}(\mathbf{x}_0)$ where \mathbf{x} is any point in the continuous three-dimensional space $(x, y, z) \in \mathbb{R}^3$ which describes the domain \mathcal{D} as a scalar field. The gradient of the scalar field will follow the ~~direction~~
150 ~~of the anisotropy~~ planar orientation of the stratigraphic structure throughout the volume or, in other words, every possible isosurface of the scalar field will represent every synchroneal deposition of the layer (see figure 2).

Let's break down what we actually mean by this: Imagine that a geological setting is formed by a perfect sequence of horizontal layers piled one above the other. If we know the exact timing of when
155 one of these surfaces was deposited, we would know that any layer above had to occur afterwards while any layer below had to be deposited earlier in time. Obviously, we cannot have data for each of these infinitesimal synchroneal layers, but we can interpolate the "date" between them. In reality, the exact year of the synchroneal deposition is ~~meaningless—since the related uncertainty would be out of~~
~~proportion~~ meaningless—as it is not possible to obtain remotely accurate estimates. What has value
160 to generate a 3D geomodel is the location of those synchroneal layers and especially the lithological

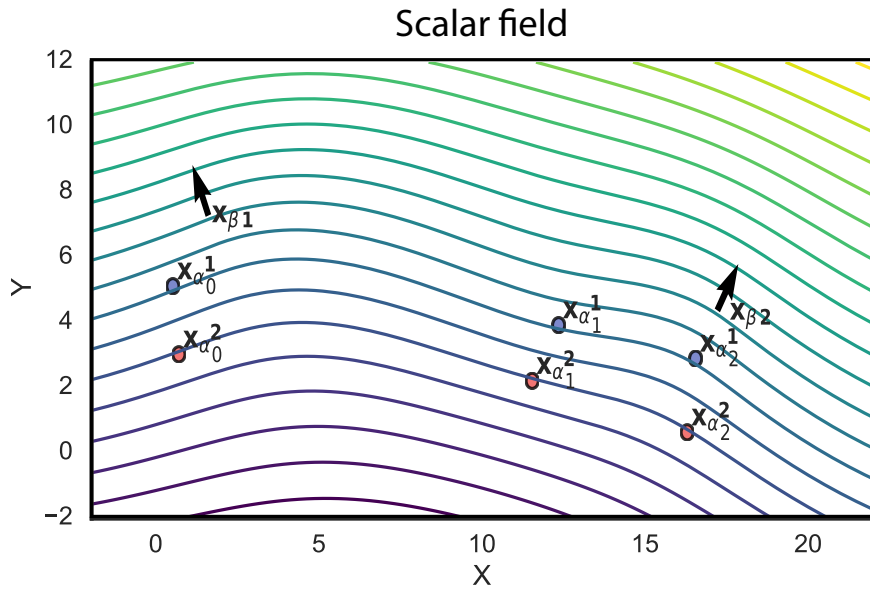


Figure 2. Example of scalar field. The input data is formed by six points distributed in two layers ($\mathbf{x}_{\alpha_i}^1$ and $\mathbf{x}_{\alpha_i}^2$) and two orientations (\mathbf{x}_{β_j}). A isosurface connect the interface points and the scalar field is perpendicular to the foliation gradient.

interfaces where the change of physical properties are notable. Due to this, instead interpolating *time*, we use a simple dimensionless parameter—that we simply refer to as *scalar field value*.

The advantages of using a global interpolator instead of interpolating each layer of interest independently are twofold: (i) the location of one layer affects the location of others in the same depositional environment, making impossible for two layers in the same potential field to cross; and
165 (ii) it enables the use of data in-between the interfaces of interest, opening the range of possible measurements that can be used in the interpolation.

The interpolation function is obtained as a weighted interpolation based on Universal CoKriging (Chiles and Delfiner, 2009). Kriging or Gaussian process regression (Matheron, 1981) is a spatial
170 interpolation that treats each input as a random variable, aiming to minimize the covariance function to obtain the best linear unbiased predictor (for a detailed description see Chapter 3 in Wackernagel, 2013). Furthermore, it is possible to combine more than one type of data—i.e. a multivariate case or CoKriging—to increase the amount of information in the interpolator, as long as we capture their relation using a cross-covariance. The main advantage in our case is to be able to utilize data
175 sampled from different locations in space for the estimation. Simple Kriging, as a regression, only minimizes the second moment of the data (or variances). However in most geological settings, we can expect linear trends in our data—i.e. the mean thickness of a layer varies across the region linearly. This trend is captured using polynomial drift functions to the system of equations in what is called Universal Kriging.

180 2.1.2 Adjustments to structural geological modeling

So far we have shown what we want to obtain and how Universal CoKriging is a suitable interpolation method to get there. In the following, we will describe the concrete steps from taking our input data to the final interpolation function $\mathbf{Z}(\mathbf{x}_0)$, ~~which describes the domain~~ where \mathbf{x}_0 refers to the estimated quantity for some integrable measure p_0 . Much of the complexity of the method comes from the difficulty of keeping highly nested nomenclature consistent across literature. For this reason, we will try to be especially verbose regarding the mathematical terminology based primarily on Chiles et al. (2004). The terms of *potential field* (original coined by Lajaunie et al., 1997) and *scalar field* (preferred by the authors) are used interchangeably across the paper. The result of a Kriging interpolation is a random function and hence both *interpolation function* and *random function* are used to refer the function of interest $\mathbf{Z}(\mathbf{x}_0)$. The CoKriging nomenclature quickly grows ~~complicated~~ convoluted, since it has to consider p random functions \mathbf{Z}_i , with p being the number of distinct parameters involved in the interpolation, sampled at different points \mathbf{x} of the three-dimensional domain \mathbb{R}^3 . Two types of parameters are used to characterize the *scalar field* in the interpolation: (i) layer interface points \mathbf{x}_α describing the respective isosurfaces of interest—usually the interface between two layers; and (ii) the gradients of the scalar field, \mathbf{x}_β —or in geological terms: poles of the layer, i.e. normal vectors to the dip plane. Therefore gradients will be oriented perpendicular to the isosurfaces and can be located anywhere in space. We will refer to the main random function—the scalar field itself— \mathbf{Z}_α simply as \mathbf{Z} , and its set of samples as \mathbf{x}_α while the second random function \mathbf{Z}_β —the gradient of the scalar field—will be referred to as $\partial\mathbf{Z}/\partial u$ with u being any unit vector and its samples as \mathbf{x}_β , ~~so that we~~. We can capture the relationship between the ~~potential~~ scalar field \mathbf{Z} and its gradient as

$$\frac{\partial \mathbf{Z}}{\partial u}(x) = \lim_{p \rightarrow 0} \frac{\mathbf{Z}(x + pu) - \mathbf{Z}(x)}{p} \lim_{\rho \rightarrow 0} \frac{\mathbf{Z}(x + u) - \mathbf{Z}(x)}{\rho} \quad (1)$$

It is also important to keep the values of every individual synchronal layer identified since they have the same scalar field value. Therefore, samples that belong to a single layer k will be expressed as a subset denoted using superscript as \mathbf{x}_α^k and every individual point by a subscript, $\mathbf{x}_{\alpha i}^k$ (see figure 2).

Note that in this context ~~data does not have any meaningful physical parameter associated with it that we want to interpolate as long as stratigraphic deposition follows gradient direction~~ the scalar field property α is dimensionless. The only limitation is that the value must increase in the direction of the gradient which in turn describes the stratigraphic deposition. Therefore the two constraints we want to conserve in the interpolated scalar field are: (i) all points belonging to a determined interface $\mathbf{x}_{\alpha i}^k$ must have the same scalar field value (i.e. there is an isosurface connecting all data points)

$$\mathbf{Z}(\mathbf{x}_{\alpha i}^k) - \mathbf{Z}(\mathbf{x}_{\alpha 0}^k) = 0 \quad (2)$$

where $\mathbf{x}_{\alpha 0}^k$ is a reference point of the interface and (ii) the scalar field will be perpendicular to the ~~poles-gradient (poles in geological nomenclature)~~ \mathbf{x}_β anywhere in 3-D space. It is important to mention that the choice of the reference points $\mathbf{x}_{\alpha 0}^k$ has no effect on the results.

Considering equation 2, we do not care about the exact value at $\mathbf{Z}(\mathbf{x}_{\alpha i}^k)$ as long as it is constant at all points $\mathbf{x}_{\alpha i}^k$. Therefore, the random function \mathbf{Z} in the CoKriging system (equation 4) can be substituted by equation 2. This formulation entails that the specific *scalar field values* will depend only on the gradients and hence at least one gradient is necessary to keep the system of equations defined. The ~~reason for this formulation rest on~~ advantage of this mathematical construction is that by not fixing the values of each interface $\mathbf{Z}(\mathbf{x}_{\alpha i}^k)$, the compression of ~~layers—which is derived by the gradients—can propagate smoother beyond the given interfaces. Otherwise, the gradients will only have effect in the area within the boundaries of layers—i.e. the two interfaces that contains the variable.~~ rate of change of the scalar field—will be only defined by the gradients $\partial \mathbf{Z} / \partial u$. This allows to propagate the effect of each gradient beyond the surrounding interfaces creating smoother formations.

The algebraic dependency between \mathbf{Z} and $\partial \mathbf{Z} / \partial u$ (equation 1) gives a mathematical definition of the relation between the two variables avoiding the need of an empirical cross-variogram, enabling instead the use of the derivation of the covariance function. This dependency must be taken into consideration in the computation of the drift of the first moment as well having a different function for each of the variables

$$\lambda F_1 + \lambda F_2 = f_{10} \quad (3)$$

where F_1 is a ~~the~~ polynomial of degree n and F_2 its derivative between the input data x_α and x_β respectively and f_{10} correspond to the same polynomial to the objective point x_0 . Having taken this into consideration, the resulting CoKriging system takes the form of:

$$\begin{bmatrix} \mathbf{C}_{\partial \mathbf{Z} / \partial \mathbf{u}, \partial \mathbf{Z} / \partial \mathbf{v}} & \mathbf{C}_{\partial \mathbf{Z} / \partial \mathbf{u}, \mathbf{Z}} & \mathbf{U}_{\partial \mathbf{Z} / \partial \mathbf{u}} \\ \mathbf{C}_{\mathbf{Z}, \partial \mathbf{Z} / \partial \mathbf{u}} & \mathbf{C}_{\mathbf{Z}, \mathbf{Z}} & \mathbf{U}_{\mathbf{Z}} \\ \mathbf{U}'_{\partial \mathbf{Z} / \partial \mathbf{u}} & \mathbf{U}'_{\mathbf{Z}} & \mathbf{0} \end{bmatrix} \begin{bmatrix} \lambda_{\partial \mathbf{Z} / \partial \mathbf{u}, \partial \mathbf{Z} / \partial \mathbf{v}} & \lambda_{\partial \mathbf{Z} / \partial \mathbf{u}, \mathbf{Z}} \\ \lambda_{\mathbf{Z}, \partial \mathbf{Z} / \partial \mathbf{u}} & \lambda_{\mathbf{Z}, \mathbf{Z}} \\ \mu_{\partial \mathbf{u}} & \mu_{\mathbf{u}} \end{bmatrix} = \begin{bmatrix} \mathbf{c}_{\partial \mathbf{Z} / \partial \mathbf{u}, \partial \mathbf{Z} / \partial \mathbf{v}} & \mathbf{c}_{\partial \mathbf{Z} / \partial \mathbf{u}, \mathbf{Z}} \\ \mathbf{c}_{\mathbf{Z}, \partial \mathbf{Z} / \partial \mathbf{u}} & \mathbf{c}_{\mathbf{Z}, \mathbf{Z}} \\ \mathbf{f}_{10} & \mathbf{f}_{20} \end{bmatrix} \quad (4)$$

where, $\mathbf{C}_{\partial \mathbf{Z} / \partial \mathbf{u}}$ is the gradient covariance-matrix; $\mathbf{C}_{\mathbf{Z}, \mathbf{Z}}$ the covariance-matrix of the differences between each interface points to reference points in each layer

$$C_{\mathbf{x}_{\alpha i}^r, \mathbf{x}_{\alpha j}^s} = C_{x_{\alpha, i}^r, x_{\alpha, j}^s} - C_{x_{\alpha, 0}^r, x_{\alpha, j}^s} - C_{x_{\alpha, i}^r, x_{\alpha, 0}^s} + C_{x_{\alpha, 0}^r, x_{\alpha, 0}^s} \quad (5)$$

(see Appendix B2 for further analysis); $\mathbf{C}_{\mathbf{Z}, \partial \mathbf{Z} / \partial \mathbf{u}}$ encapsulates the cross-covariance function; and $\mathbf{U}_{\mathbf{Z}}$ and $\mathbf{U}'_{\partial \mathbf{Z} / \partial \mathbf{u}}$ are the drift functions and their gradient, respectively. On the right hand side we find the ~~vector of the matrix system of equations~~ matrix of independent terms, being $\mathbf{c}_{\partial \mathbf{Z} / \partial \mathbf{u}, \partial \mathbf{Z} / \partial \mathbf{v}}$ the gradient of the covariance function to the point \mathbf{x} of interest; $\mathbf{c}_{\mathbf{Z}, \partial \mathbf{Z} / \partial \mathbf{u}}$ the cross-covariance; $\mathbf{c}_{\mathbf{Z}, \mathbf{Z}}$ the actual covariance function; and \mathbf{f}_{10} and \mathbf{f}_{20} the gradient of the drift functions and the drift

functions themselves. Lastly, the unknown vectors are formed by the corresponding weights, λ , and constants of the drift functions, μ . A more detail inspection of this system of equations is carried out in Appendix B.

As we can see in equation 4, it is possible to solve the Kriging system for the scalar field \mathbf{Z} (second column in the weights vector), as well as its derivative $\partial\mathbf{Z}/\partial u$ (first column in the weights vector).

Even though the main goal is the segmentation of the layers, which is done using the value of \mathbf{Z} (see Section 2.2.1), the gradient of the scalar field can be used for further mathematical applications, such as meshing, geophysical forward calculations or locating geological structures of interest (e.g. spill points of a hydrocarbon trap).

Furthermore, since the choice of covariance parameters is ad hoc (Appendix D show the used covariance function in GemPy), the uncertainty derived by the Kriging interpolation does not bear any physical meaning. This fact promotes the idea of only using the mean value of the Kriging solution. For this reason it is recommended to solve the Kriging system (equation 4) in its dual form (Matheron, 1981, see Appendix C).

2.2 Geological model interpolation using *GemPy*

2.2.1 From scalar field to geological block model

In most scenarios the goal of structural modeling is to define the spatial distribution of geological structures, such as layers interfaces and faults. In practice, this segmentation usually is done either by using a volumetric discretization or by depicting the interfaces as surfaces.

The result of the Kriging interpolation is the random function $\mathbf{Z}(x)$ (and its gradient $\partial\mathbf{Z}/\partial u(x)$, which we will omit in the following), which allows the evaluation of the value of the scalar field at any given point x in space. From this point on, the easiest way to segment the domains is to discretize the 3-D space (e.g. we use a regular grid in figure 3). First, we need to calculate the scalar value at every interface by computing $\mathbf{Z}(\mathbf{x}_{\alpha,i}^k)$ for every interface k_i . Once we know the value of the scalar field at the interfaces, we evaluate every point of the mesh and compare their value to those at the interfaces, identifying every point of the mesh with a topological volume. Each of these compartmentalizations will represent each individual domain, this is, each lithology of interest (see figure 3a).

At the time of this manuscript preparation, *GemPy* only provides rectilinear grids but it is important to notice that the computation of the scalar field happens in continuous space, and therefore allows the use of any type of mesh. The result of this type of segmentation is referred in *GemPy* as a *lithology block*.

The second segmentation alternative consist on locating the layer isosurfaces. *GemPy* makes use of the marching cube algorithm (Lorensen and Cline, 1987) provided by the *scikit-image* library (van der Walt et al., 2014). The basics of the marching cube algorithm are quite intuitive: (i) First, we

280 discretize the volume in 3-D voxels and by comparison we look if the value of the isosurface we want to extract falls within the boundary of every single voxel; (ii) if so, for each edge of the voxel, we interpolate the values at the corners of the cube to obtain the coordinates of the intersection between the edges of the voxels and the isosurface of interest, commonly referred to as vertices; (iii) those intersections are analyzed and compared against all possible configurations to define the simplices (i.e. 285 the vertices which form an individual polygon) of the triangles. Once we obtain the coordinates of vertices and their correspondent simplices, we can use them for visualization (see Section 3.1) or any sub-sequential computation that may make use of them (e.g. weighted voxels). For more information on meshing algorithms refer to ~~(Geuzaine and Remacle, 2009)~~[Geuzaine and Remacle \(2009\)](#).

Listing 1. Code to generate a single scalar field model (as seen in figure 2) and plotting a section of a regular grid (figure 3a) and extracting surfaces points at the interfaces.

```
290 import gempy as gp

# Main data management object containing
geo_data = gp.create_data(extent=[0, 20, 0, 10, -10, 0],
                          resolution=[100, 10, 100],
295                          path_o="paper_Foliations.csv",
                          path_i="paper_Points.csv")

# Creating object with data prepared for interpolation and compiling
interp_data = gp.InterpolatorData(geo_data)

300 # Computing result
lith, fault = gp.compute_model(interp_data)

# Plotting result: scalar field
305 gp.plot_scalar_field(geo_data, lith[1], 5, plot_data=True)

# Plotting result: lithology block
gp.plot_section(geo_data, lith[0], 5, plot_data=True)

310 # Getting vertices and faces
vertices, simplexes = gp.get_surfaces(interp_data, lith[1], [fault[1]], original_scale=True)
```

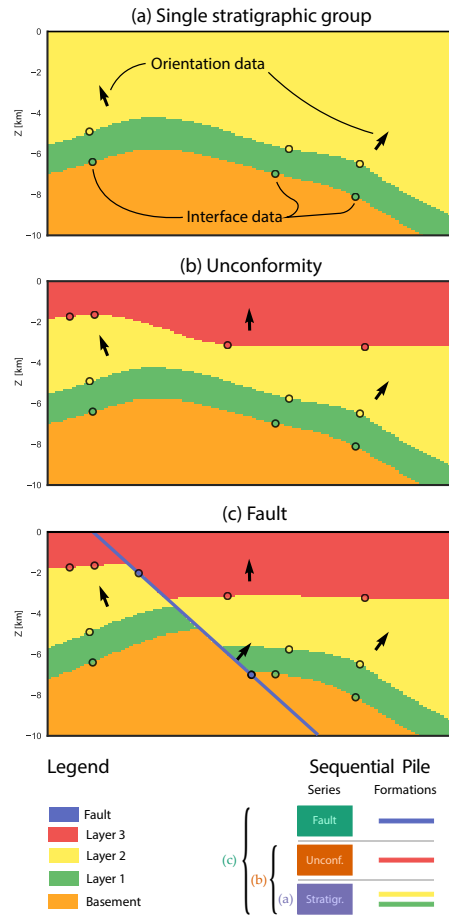


Figure 3. Example of different lithological units and their relation to scalar fields. a) Simple stratigraphic sequence generated from a scalar field as product of the interpolation of interface points and orientation gradients. b) Addition of an unconformity horizon from which the unconformity layer behaves independently from the older layers by overlying a second scalar field. c) Combination of unconformity and faulting using three scalar fields.

2.2.2 Combining scalar fields: Depositional series and faults

In reality, most geological settings are formed by a concatenation of depositional phases partitioned by unconformity boundaries and subjected to tectonic stresses which displace and deform the layers. While the interpolation is able to represent realistic folding—given enough data—the method fails to describe discontinuities. To overcome this limitation, it is possible to combine several scalar fields to recreate the desired result.

So far the implemented discontinuities in *GemPy* are unconformities and infinite faults. Both types are computed by specific combinations of independent scalar fields. We call these independent scalar fields *series* (from stratigraphic series in accordance to the use in GeoModeller 3-D Calcagno et al., 2008) and in essence, they represent a subset of grouped interfaces—either layers or fault planes—

that are interpolated together and therefore their spatial location affect each other. To handle and visualize these relationships, we use a so called sequential pile; representing the order—from the first scalar field to the last—and the grouping of the layers (see figure 3). It is interesting to point out that the sequential pile only controls the order of each individual series. Within each series, the stratigraphic sequence is strictly determined by the geometry and the interpolation algorithm.

Modeling unconformities is rather straightforward. Once we have grouped the layers into their respective series, younger series will overlay older ones beyond the unconformity. The scalar fields themselves, computed for each of these series, could be seen as a continuous depositional sequence in the absence of an unconformity.

Listing 2. Extension of the code in Listing 1 to generate an unconformity by using two scalar fields. The corresponding model is shown in figure 3b)

```
import gempy as gp

# Main data management object containing
geo_data = gp.create_data(extent=[0, 20, 0, 10, -10, 0],
                          resolution=[100, 10, 100],
                          path_o="paper_Foliations.csv",
                          path_i="paper_Points.csv")

# Defining the series of the sequential pile
gp.set_series(geo_data,
              {'younger_series' : 'Unconformity', 'older_series': ('Layer1', 'Layer2')},
              order_formation= ['Unconformity', 'Layer2', 'Layer1'])

# Creating object with data prepared for interpolation and compiling
interp_data = gp.InterpolatorData(geo_data)

# Computing result
lith, fault = gp.compute_model(interp_data)

# Plotting result
gp.plot_section(geo_data, lith[0], 5, plot_data=True)
```

Faults are modeled by the inclusion of an extra drift term into the kriging system (Marechal, 1984):

$$\begin{bmatrix} \mathbf{C}_{\partial \mathbf{Z} / \partial \mathbf{u}, \partial \mathbf{Z} / \partial \mathbf{v}} & \mathbf{C}_{\partial \mathbf{Z} / \partial \mathbf{u}, \mathbf{Z}} & \mathbf{U}_{\partial \mathbf{Z} / \partial \mathbf{u}} & \mathbf{F}_{\partial \mathbf{Z} / \partial \mathbf{u}} \\ \mathbf{C}_{\mathbf{Z}, \partial \mathbf{Z} / \partial \mathbf{u}} & \mathbf{C}_{\mathbf{Z}, \mathbf{Z}} & \mathbf{U}_{\mathbf{Z}} & \mathbf{F}_{\mathbf{Z}} \\ \mathbf{U}'_{\partial \mathbf{Z} / \partial \mathbf{u}} & \mathbf{U}'_{\mathbf{Z}} & \mathbf{0} & \mathbf{0} \\ \mathbf{F}'_{\partial \mathbf{Z} / \partial \mathbf{u}} & \mathbf{F}'_{\mathbf{Z}} & \mathbf{0} & \mathbf{0} \end{bmatrix} \begin{bmatrix} \lambda_{\partial \mathbf{Z} / \partial \mathbf{u}, \partial \mathbf{Z} / \partial \mathbf{v}} & \lambda_{\partial \mathbf{Z} / \partial \mathbf{u}, \mathbf{Z}} \\ \lambda_{\mathbf{Z}, \partial \mathbf{Z} / \partial \mathbf{u}} & \lambda_{\mathbf{Z}, \mathbf{Z}} \\ \mu_{\partial \mathbf{u}} & \mu_{\mathbf{u}} \\ \mu_{\partial \mathbf{f}} & \mu_{\mathbf{f}} \end{bmatrix} = \begin{bmatrix} \mathbf{c}_{\partial \mathbf{Z} / \partial \mathbf{u}, \partial \mathbf{Z} / \partial \mathbf{v}} & \mathbf{c}_{\partial \mathbf{Z} / \partial \mathbf{u}, \mathbf{Z}} \\ \mathbf{c}_{\mathbf{Z}, \partial \mathbf{Z} / \partial \mathbf{u}} & \mathbf{c}_{\mathbf{Z}, \mathbf{Z}} \\ \mathbf{f}_{10} & \mathbf{f}_{20} \\ \mathbf{f}_{10} & \mathbf{f}_{20} \end{bmatrix} \quad (6)$$

which is a function of the faulting structure. This means that for every location \mathbf{x}_0 the drift function will take a value depending on the fault compartment—i.e. a segmented domain of the fault network—and other geometrical constrains such as spatial influence of a fault or variability of the offset. To obtain the offset effect of a fault, the value of the drift function has to be different at each

of its sides. The level of complexity of the drift functions will determine the quality of the characterization as well as its robustness. Furthermore, finite or localized faults can be recreated by selecting an adequate function that describes those specific trends.

Listing 3. Code to generate a model with an unconformity and a fault using a three scalar fields model (as seen in figure 3c) and the visualization 3D using vtk (see figure 5).

```

365 import gempy as gp

# Main data management object containing \DIFaddbegin \DIFadd{the location of all interfaces
# and orientations parameters as well as the formation/fault to which belong
370 }\DIFaddend geo_data = gp.create_data(extent=[0,20,0,10,-10,0],
                                     resolution=[100,10,100],
                                     path_o = "paper_Foliations.csv",
                                     path_i = "paper_Points.csv")

375 # Defining the series of the sequential pile\DIFaddbegin \DIFadd{. This is done by
# categorizing interfaces and orientations by its formation label
}\DIFaddend gp.set_series(geo_data, series_distribution={'fault_series1': 'fault1',
                                     'younger_series' : 'Unconformity',
                                     'older_series': ('Layer1', 'Layer2')},
380 order_formation= ['fault1', 'Unconformity', 'Layer2', 'Layer1'])

# Creating object with data prepared for interpolation and compiling
interp_data = gp.InterpolatorData(geo_data)

385 # Computing result
lith, fault = gp.compute_model(interp_data)

# Plotting result
gp.plot_section(geo_data, lith[0], 5, plot_data=True)
390

# Getting vertices and faces and plotting
vertices, simplexes = gp.get_surfaces(interp_data, lith[1], [fault[1]], original_scale=True)
gp.plot_surfaces_3D(geo_data, ver_s, sim_s)

```

395 The computation of the segmentation of fault compartments (called *fault block* in *GemPy*)—prior to the inclusion of the fault drift functions which depends on this segmentation—can be performed with the potential-field method itself. In the case of multiple faults, individual drift functions have to be included in the kriging system for each fault, representing the subdivision of space that they produce. Naturally, younger faults may offset older tectonic events. This ~~behaviour~~behavior is replicated
400 by recursively adding drift functions of younger faults to the computation of the older *fault blocks*. To date, the fault relations—i.e. which faults offset others—is described by the user in a boolean matrix. An easy to use implementation to generate fault networks is being worked on at the time of the manuscript preparation.

An important detail to consider is that drift functions will bend the isosurfaces according to the
405 given rules but they will conserve their continuity. This differs from the intuitive idea of offset, where the interface presents a sharp jump. This fact has direct impact in the geometry of the final model, and can, for example, affect certain meshing algorithms. Furthermore, in the ideal case of

choosing the perfect drift function, the isosurface would bend exactly along the faulting plane. At the current state *GemPy* only includes the addition of an arbitrary integer to each segmented volume.

410 This limits the quality to a constant offset, decreasing the sharpness of the offset as data deviates from that constrain. Any deviation from this theoretical concept, results in a bending of the layers as they approximate the fault plane to accommodate to the data, potentially leading to overly smooth transitions around the discontinuity.

2.3 "Under the hood": The *GemPy* architecture

415 2.3.1 The graph structure

The architecture of *GemPy* follows the Python Software Foundation recommendations of modularity and reusability (van Rossum et al., 2001). The aim is to divide all functionality into independent small logical units in order to avoid duplication, facilitate readability and make changes to the code base easier.

420 ~~The design of *GemPy* revolves around~~ 's architecture was design from the ground up to accommodate
an automatic differentiation (AD) ~~sehemelibrary~~. The main constraint is that the mathematical func-
tions need to be continuous from the ~~input parameters variables~~ (in probabilistic jargon priors) to the
cost function (or likelihoods), and therefore the code must be written in the same language (or at the
very least compatible) to automatically compute the derivatives. In practice, this entails that any oper-
425 ation involved in the AD must be coded symbolically using the library *Theano* (see Section 2.3.2 for
further details). ~~One of the constrains of writing symbolically is the~~ Writing symbolically requires
a priori declaration of ~~the possible input parameters of the graph all algebra, from variables~~ which
will behave as latent ~~variables—iparameters—~~i.e. the parameters we try to tune for optimization
or uncertainty ~~quantification—while leaving others involved parameters constant either due to their~~
430 ~~nature or because of the relative slight impact of their variability. This rigidity~~ quantification—to
all involved constants and the specific mathematical functions that relates them. This statements
generate a so called graph that encapsulates symbolically all the logic what enables to perform
further analysis on the logic itself (e.g. differentiation or optimization). However the rigidity when
constructing the graph dictates the whole design of input data management~~that needs to revolved~~
435 ~~around the preexistent symbolie graph.~~

GemPy encapsulates this creation of the symbolic graph in its the module `theanograph`. Due to the significant complexity to program symbolically, features shipped in *GemPy* that rely heavily in external libraries are not written in *Theano* yet. The current functionality written in *Theano* can be seen in the figure 4 and essentially it encompasses all the interpolation of the geological modeling
440 (section 2.1) as well as forward calculation of the gravity (section 3.2).

Regarding data structure, we make use of the Python package *pandas* (McKinney, 2011) to store and prepare the input data for the symbolic graph (red nodes in figure 4) or other processes, such as

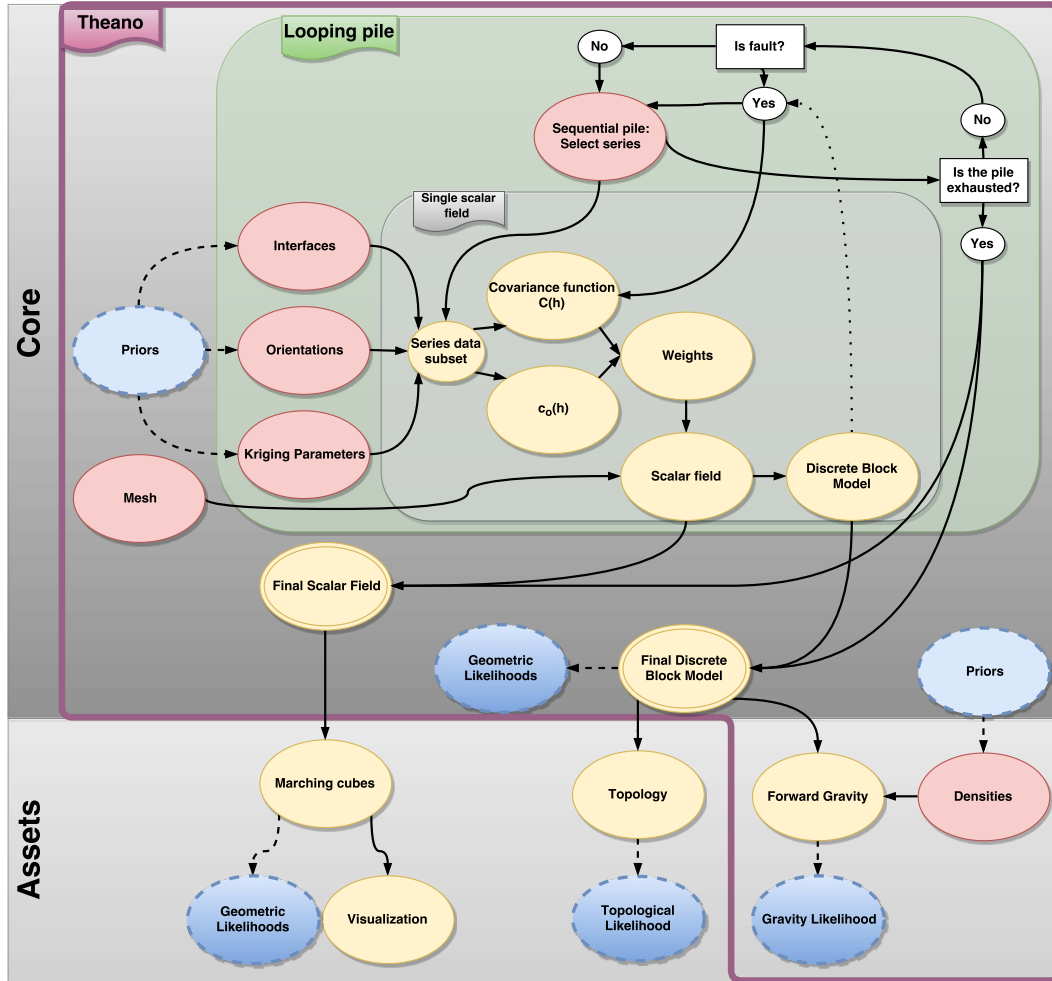


Figure 4. Graph of the logical structure of *GemPy* logic. There are several levels of abstraction represented. (i) The first division is between the implicit interpolation of the geological modeling (dark gray) and other subsequent operations for different objectives (light gray). (ii) All the logic required to perform automatic differentiation is presented under the “Theano” label (in purple) (iii) The parts under labels “Looping pile” (green) and “Single potential field” (gray), divide the logic to control the input data of each necessary scalar field and the operations within one of them. (iv) Finally, each superset of parameters is color coded according to their probabilistic nature and behavior in the graph: in blue, stochastic variables (priors or likelihoods); in yellow, deterministic functions; and in red the inputs of the graph, which are either stochastic or constant depending on the problem.

visualization. All the methodology to create, export and manipulate the original data is encapsulated in the class `DataManagement`. This class has several child classes to facilitate specific precomputation manipulations of data structures (e.g. for meshing). The aim is to have all constant data prepared before any inference or optimization is carried out to minimize the computational overhead of each iteration as much as possible.

It is important to keep in mind that, in this structure, once data enters the part of the symbolic graph, only algebraic operations are allowed. This limits the use of many high-level coding structures (e.g. dictionaries or undefined loops) and external dependencies. As a result of that, the preparation of data must be exhaustive before starting the computation. This includes ordering the data within the arrays, passing the exact lengths of the subsets we will need later on during the interpolation or the calculation of many necessary constant parameters. The preprocessing of data is done within the sub-classes of `DataManagement`, the `InterpolatorData` class—of which an instance is used to call the *Theano* graph—and `InterpolatorClass`—which creates the *Theano* variables and compiles the symbolic graph.

The rest of the package is formed by—an always growing—series of modules that perform different tasks using the geological model as input (see Section 3 and the assets-area in figure 4).

2.3.2 Theano

Efficiently solving a large number of algebraic equations, and especially their derivatives, can easily get unmanageable in terms of both time and memory. Up to this point we have referenced many times *Theano* and its related terms such as automatic differentiation or symbolic programming. In this section we will motivate its use and why its capabilities make all the difference in making implicit geological modeling available for uncertainty analysis.

Theano is a Python package that takes over many of the optimization tasks in order to create a computationally feasible code implementation. *Theano* relies on the creation of symbolical graphs that represent the mathematical expressions to compute. Most of the extended programming paradigms (e.g. procedural languages and object-oriented programming; see Normark, 2013) are executed sequentially without any interaction with the subsequent instructions. In other words, a later instruction has access to the memory states but is clueless about the previous instructions that have modified mentioned states. In contrast, symbolic programming define from the beginning to the end not only the primary data structure but also the complete logic of a function, which in turn enables the optimization (e.g. redundancy) and manipulation (e.g. derivatives) of its logic.

Within the Python implementation, *Theano* create an acyclic network graph where the parameters are represented by nodes, while the connections determine mathematical operators that relate them. The creation of the graph is done in the class `theanograph`. Each individual method corresponds to a piece of the graph starting from the input data all the way to the geological model or the forward gravity (see figure 4, purple Theano area).

The symbolic graph is later analyzed to perform the optimization, the symbolic differentiation
 480 and the compilation to a faster language than Python (C or CUDA). This process is computational
 demanding and therefore it must be avoided as much as possible.

Among the most outstanding optimizers shipped with *Theano* (for a detailed description see
 Theano Development Team, 2016), we can find : (i) the canonicalization of the operations to re-
 duce the number of duplicated computations, (ii) specialization of operations to improve consecutive
 485 element-wise operations, (iii) in-place operations to avoid duplications of memory or (iv) Open MP
 parallelization for CPU computations. These optimizations and more can speed up the code an order
 of magnitude.

However, although *Theano* code optimization is useful, the real game-changer is its capability to
 perform automatic differentiation. There is extensive literature explaining ~~all the ins and outs and~~
 490 ~~intuitions of the method~~ in detail the method and its related intuitions since it is a core algorithm
 to train neural networks (e.g. a detailed explanation is given by Baydin et al., 2015). Here, we will
 highlight the main differences with numerical approaches and how they can be used to improve the
 modeling process.

Many of the most advanced algorithms in computer science rely on an inverse framework i.e. the
 495 result of a forward computation $f(\mathbf{x})$ influences the value of one or many of the \mathbf{x} latent variables (e.g.
 neuronal networks, optimizations, inferences). The most emblematic example of this is the optimiza-
 tion of a cost function. All these problems can be described as an exploration of a multidimensional
 manifold $f : \mathbb{R}^N \rightarrow \mathbb{R}$. Hence the gradient of the function $\nabla f = \left(\frac{\partial f}{\partial x_1}, \frac{\partial f}{\partial x_2}, \dots, \frac{\partial f}{\partial x_n} \right)$ becomes key
 for an efficient analysis. In case that the output is also multidimensional—i.e. $f : \mathbb{R}^N \rightarrow \mathbb{R}^M$ —the
 500 entire manifold gradient can be expressed by the Jacobian matrix

$$Jf = \begin{bmatrix} \frac{\partial f_1}{\partial x_1} & \cdots & \frac{\partial f_1}{\partial x_n} \\ \vdots & \ddots & \vdots \\ \frac{\partial f_m}{\partial x_1} & \cdots & \frac{\partial f_m}{\partial x_n} \end{bmatrix} \quad (7)$$

of dimension $N \cdot M$, where N is the number of variables and M the number of functions that de-
 pend on those variables. Now the question is how we compute the Jacobian matrix in a consistent
 and efficient manner. The most straightforward methodology consists in approximating the derivate
 505 by numerical differentiation applying finite differences approximations, for example a forward FD
 scheme:

$$\frac{\partial f_i}{\partial x_i} = \lim_{h \rightarrow 0} \frac{f(x_i + h) - f(x_i)}{h} \quad (8)$$

where h is a discrete increment. The main advantage of numerical differentiation is that it only
 computes f —evaluated for different values of x —which makes it very easy to implement it in any
 510 available code. By contrast, a drawback is that for every element of the Jacobian we are introducing
 an approximation error that eventually can lead to mathematical instabilities. But above all, the main

limitation is the need of $2 \cdot M \cdot N$ evaluations of the function f , which quickly becomes prohibitively expensive to compute in high-dimensional problems.

The alternative is to create the symbolic differentiation of f . This encompasses decomposing f into its primal operators and applying the chain rule to the correspondent transformation by following the rules of differentiation to obtain f' . However, symbolic differentiation is not enough since the application of the chain rule leads to exponentially large expressions of f' in what is known as "expression swell" (Cohen, 2003). Luckily, these large symbolic expressions have a high level of redundancy in their terms. This allows to exploit this redundancy by storing the repeated intermediate steps in memory and simply invoke them when necessary, instead of computing the whole graph every time. This division of the program into sub-routines to store the intermediate results—which are invoked several times—is called dynamic programming (Bellman, 2013). The simplified symbolic differentiation graph is ultimately what is called automatic differentiation (Baydin et al., 2015). Additionally, in a multivariate/multi-objective case the benefits of using AD increase linearly as the difference between the number of parameters N and the number of objective functions M get larger. By applying the same principle of redundancy explained above—this time between intermediate steps shared across multiple variables or multiple objective function—it is possible to reduce the number of evaluations necessary to compute the Jacobian either to N in forward-propagation or to M in back-propagation, plus a small overhead on the evaluations (for a more detailed description of the two modes of AD see Cohen, 2003).

Theano provides a direct implementation of the back-propagation algorithm, which means in practice that a new graph of similar size is generated per cost function (or, in the probabilistic inference, per likelihood function, [see 3.4 for more detail](#)). Therefore, the computational time is independent of the number of input parameters, opening the door to solving high-dimensional problems.

3 ASSETS – Model analysis and further use

In this second half of the paper we will explore different features that complement and expand the construction of the geological model itself. These extensions are just some examples of how *GemPy* can be used as geological modeling engine for diverse research projects. The numerous libraries in the open-source ecosystem allow to choose the best narrow purpose tool for very specific tasks. Considering the visualization of *GemPy*, for instance: *matplotlib* (Hunter, 2007) for 2-D visualization, *vtk* for fast and interactive 3-D visualization, *steno3D* for sharing block models visualizations online—or even the open-source 3-D modeling software Blender (Blender Online Community, 2017) for creating high quality renderings and Virtual Reality, are only some examples of the flexibility that the combination of *GemPy* with other open-source packages offers. In the same fashion we can use the geological model as basis for the subsequent geophysical simulations and process simulations. Due to Python's modularity, combining distinct modules to extend the scope of a project to include

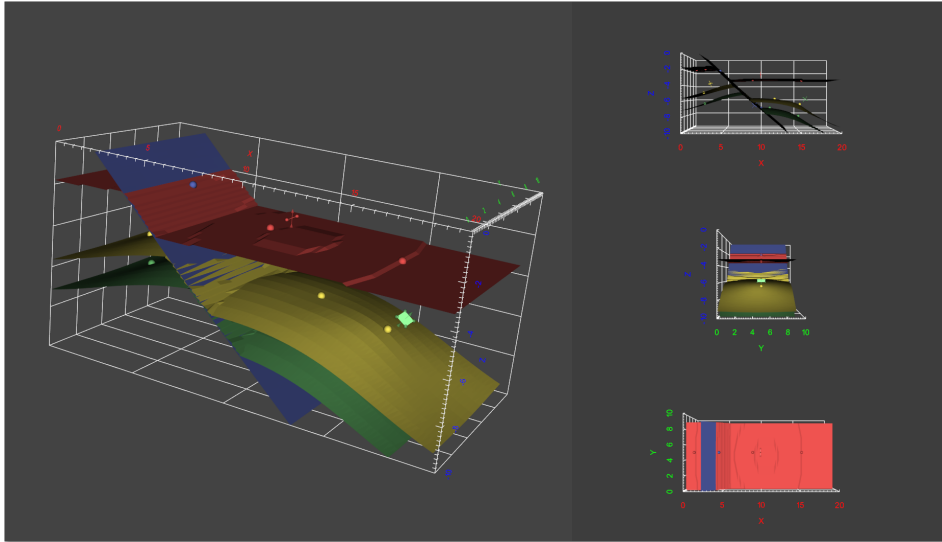


Figure 5. In-built *vtk* 3-D visualization of *GemPy* provides an interactive visualization of the geological model (left) and three additional orthogonal viewpoints (right) from different directions.

the geological modeling process into a specific environment is effortless. In the next sections we will dive into some of the built-in functionality implemented to date on top of the geological modeling core. Current assets are: (i) 2-D and 3-D visualizations, (ii) forward calculation of gravity, (iii) topology analysis, (iv) uncertainty quantification (UQ) as well as (v) full Bayesian inference.

3.1 Visualization

The segmentation of meaningful units is the central task of geological modelling. It is often a prerequisite for engineering projects or process simulations. An intuitive 3-D visualization of a geological model is therefore a fundamental requirement.

For its data and model visualization, *GemPy* makes use of freely available tools in the Python module ecosystem to allow the user to inspect data and modeling results from all possible angles. The fundamental plotting library *matplotlib* (Hunter, 2007), enhanced by the statistical data visualization library *seaborn* (Waskom et al., 2017), provides the 2-D graphical interface to visualize input data and 2-D sections of scalar fields and geological models. In addition, making use of the capacities of *pyqt* implemented with *matplotlib*, we can generate interactive sequence piles, where the user can not only visualize the temporal relation of the different unconformities and faulting events, but also modify it using intuitive drag and drop functionality (see figure 5).

On top of these features, *GemPy* offers in-built 3-D visualization based on the the open-source Visualization Toolkit (VTK Schroeder et al., 2004). It provides users with an interactive 3-D view of the geological model, as well as three additional orthogonal viewpoints (see figure 5). The user can decide to plot just the data, the geological surfaces, or both. In addition to just visualizing the

data in 3-D, *GemPy* makes use of the interaction capabilities provided by *vtk* to allow the user to move input data points on the fly via drag-and-drop. Combined with *GemPy*'s optimized modeling process (and the ability to use GPUs for efficient model calculation), this feature allows for data modification with real-time updating of the geological model (in the order of milliseconds per scalar field). This functionality can not only improve the understanding of the model but can also help the user to obtain the desired outcome by working directly in 3-D space while getting direct visual feedback on the modeling results. Yet, due to the exponential increase of computational time with respect to the number of input data and the model resolution), very large and complex models may have difficulties to render fast enough to perceive continuity on conventional computer systems.

For additional high quality visualization, we can generate *vtk* files using *pyevtk*. These files can later be loaded into external VTK viewer as Paraview (Ayachit, 2015) in order to take advantage of its intuitive interface and powerful visualization options. Another natural compatibility exists with Blender (Blender Online Community, 2017) due to its use of Python as front-end. Using the Python distribution shipped within a Blender installation, it is possible to import, run and automatically represent *GemPy*'s data and results (figure 1, see appendix F for code extension). This not only allow to render high quality images and videos but also to visualize the models in Virtual Reality, making use of the Blender Game engine and some of the plug-ins that enable this functionality.

For sharing models, *GemPy* also includes functionality to upload discretized models to the Steno 3D platform (a freemium business model). Here, it is possible to visualize manipulate and shared the model with any number of people effortlessly by simple invitations or the distribution of a link.

In short, *GemPy* is not limited to a unique visualization library. Currently *GemPy* gives support to many of the available visualization options to fulfill the different needs of the developers accordingly. However, these are not by all means the only possible alternatives and in the future we expect that *GemPy* to be employed as backend of other *further* projects.

3.2 Gravity forward modeling

In recent years gravity measurements has increased in quality (Nabighian et al., 2005) and is by now a valuable additional geophysical data source to support geological modeling. There are different ways to include the new information into the modeling workflow, and one of the most common is via inversions (Tarantola, 2005). Geophysics can validate the quality of the model in a probabilistic or optimization framework but also by back-propagating information, geophysics can improve automatically the modeling process itself. As a drawback, simulating forward geophysics adds a significant computational cost and increases the uncertainty to the parametrization of the model. However, due to the amount of uncorrelated information—often continuous in space—the inclusion of geophysical data in the modeling process usually becomes significant to evaluate the quality of a given model.

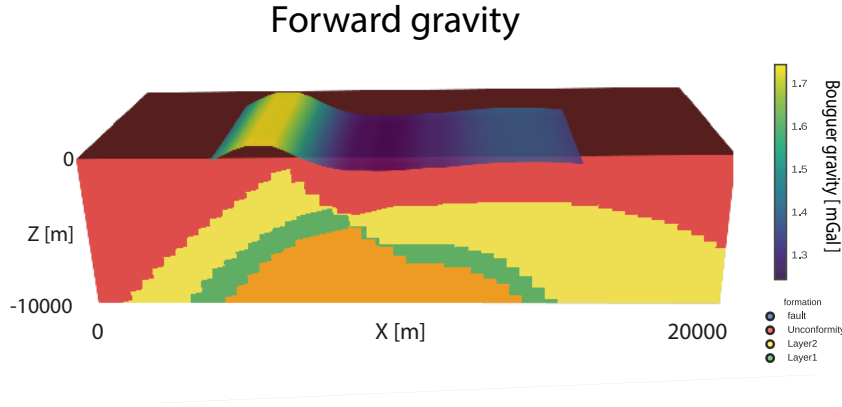


Figure 6. Forward gravity response overlaid on top of a ~~XY cross section of the 3-D~~ lithology ~~block~~ sliced on the Y direction.

GemPy includes built-in functionality to compute forward gravity conserving the automatic differentiation of the package. It is calculated from the discretized block model applying the method of Nagy (1966) for rectangular prisms in the z direction,

$$F_z = G_\rho \left[x \ln(y+r) + y \ln(x+r) - z \arctan\left(\frac{xy}{zr}\right) \right]_{x_1|y_1|z_1}^{x_2|y_2|z_2} \quad (9)$$

where x , y , and z are the Cartesian components from the measuring point of the prism, r the euclidean distance and G_ρ the average gravity pull of the prism. This integration provides the gravitational pull of every voxel for a given density and distance in the component z . Taking advantage of the immutability of the involved parameters with the exception of density allow us to precompute the decomposition of t_z , ~~leaving~~ i.e. the distance dependent side of Equation 9 ~~leaving~~ just its product with the weight G_ρ

$$F_z = G_\rho \cdot t_z \quad (10)$$

as a recurrent operation.

As an example, we show here the forward gravity response of the geological model in figure 3c. The first important detail is the increased extent of the interpolated model to avoid boundary errors. In general, a padding equal to the maximum distance used to compute the forward gravity computation would be the ideal value. In this example (figure 6) we ~~add~~ 10 km to the X and Y coordinates. The next step is to define the measurement 2-D grid—i.e. where to simulate the gravity response and the densities of each layers. The densities chosen are: 2.92, 3.1, 2.61 and 2.92 kg/m³ for the basement, "Unconformity" layer (i.e. the layer on top of the unconformity), Layer 1 and Layer 2 respectively.

Listing 4. Computing forward gravity of a *GemPy* model for a given 2-D grid (see figure 6).

```
import matplotlib.pyplot as plt
```

```

import gempy as gp
625
# Main data management object containing. The extent must be large enough respect the forward
# gravity plane to account the effect of all cells at a given distance, $d$ to any spatial
# direction $x, y, z$.
geo_data = gp.create_data(extent=[-10,30,-10,20,-10,0],
630
                        resolution=[50,50,50],
                        path_o = "paper_Foliations.csv",
                        path_i = "paper_Points.csv")

# Defining the series of the sequential pile
635 gp.set_series(geo_data, series_distribution={'fault_seriel': 'fault1',
                                             'younger_serie' : 'Unconformity',
                                             'older_serie': ('Layer1', 'Layer2')},
               order_formation= ['fault1', 'Unconformity', 'Layer2', 'Layer1'])

640 # Creating object with data prepared for interpolation and compiling.
interp_data = gp.InterpolatorData(geo_data, output='gravity')

# Setting the 2D grid of the airborne where we want to compute the forward gravity
gp.set_geophysics_obj(interp_data_g, ai_extent = [0, 20, 0, 10, -10, 0],
645
                    ai_resolution = [30,10])

# Making all possible precomputations: Decomposing the value tz for every point of the 2D grid
# to each voxel
gp.precomputations_gravity(interp_data_g, 25, densities=[2.92, 3.1, 2.61, 2.92])
650

# Computing gravity (Eq. 10)
lith, fault, grav = gp.compute_model(interp_data_g, 'gravity')

# Plotting lithology section
655 gp.plot_section(geo_data, lith[0], 0, direction='z', plot_data=True)

# Plotting forward gravity
plt.imshow(grav.reshape(10,30), cmap='viridis', origin='lower', alpha=0.8, extent=[0,20,0,10])

```

660 The computation of forward gravity is a required step towards a fully coupled gravity inversion. Embedding this step into a Bayesian inference allows to condition the initial data used to create the model to the final gravity response. This idea will be further developed in Section 3.4.2.

3.3 Topology

The concept of topology provides a useful tool to describe adjacency relations in geomodels, such as stratigraphic contacts or across-fault connectivity (for a more detailed introduction see Thiele et al., 2016a, b). *GemPy* has in-built functionality to analyze the adjacency topology of its generated models as Region Adjacency Graphs (RAGs), using the `topology_compute` method (see Listing 6). It can be directly visualized on top of model sections (see figure 7), where each unique topological region in the geomodel is represented by a graph node, and each connection as a graph edge. The function outputs the graph object `G`, the region centroid coordinates, a list of all the unique node labels, and two look-up tables to conveniently reference node labels and lithologies

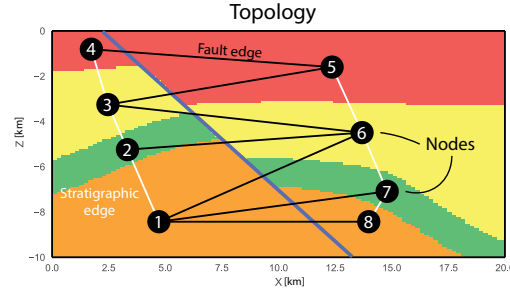


Figure 7. Section of the example geomodel with overlaid topology graph. The geomodel contains eight unique regions (graph nodes) and 13 unique connections (graph edges). White edges represent stratigraphic and unconformity connections, while black edges correspond to across-fault connections.

To analyze the model topology, *GemPy* makes use of a general connected component labeling (CCL) algorithm to uniquely label all separated geological entities in 3-D geomodels. The algorithm is provided via the widely used, open-source, Python-based image processing library *scikit-image* (Van der Walt et al., 2014) by the function `skimage.measure.label`, which is based on the optimized algorithms of (Fiorio and Gustedt, 1996; Wu et al., 2005). But just using CCL on a 3-D geomodel fails to discriminate a layer cut by a fault into two unique regions because in practice both sides of a fault are represented by the same label. To achieve the detection of edges across the fault, we need to precondition the 3-D geomodel matrix, which contains just the lithology information (layer id), with a 3-D matrix containing the information about the faults (fault block id). We multiply the binary fault array (0 for foot wall, 1 for hanging wall) with the maximum lithology value incremented by one. We then add it to the lithology array to make sure that layers that are in contact across faults are assigned a unique integer in the resulting array. This yields a 3-D matrix which combines the lithology information and the fault block information. This matrix can then be successfully labeled using CCL with a 2-connectivity stamp, resulting in a new matrix of uniquely labeled regions for the geomodel. From these, an adjacency graph is generated using `skimage.future.graph.RAG`, which created a Region Adjacency Graph (RAG) of all unique regions contained in a 2-D or 3-D matrix, representing each region with a node and their adjacency relations as edges, successfully capturing the topology information of our geomodel. The connections (edges) are then further classified into either stratigraphic or across-fault edges, to provide further information. If the argument `compute_areas=True` was given, the contact area for the two regions of an edge is automatically calculated (number of voxels) and stored inside the adjacency graph.

Listing 5. Topology analysis of a *GemPy* geomodel.

```
...
Add Listing 3
...

# Computing result
```

```

700 lith, fault = gp.compute_model(interp_data)

    # Compute topology
    G, centroids, labels_unique, labels_lot, lith_lot = gp.topology_compute(geo_data, lith[0],
        fault[0], compute_areas=True)
705

    # Plotting topology network
    gp.plot_section(geo_data, lith[0], 5)
    gp.topology_plot(geo_data, G, centroids)

```

710 3.4 Stochastic Geomodeling and probabilistic programming

Raw geological data is noisy and measurements are usually sparse. As a result, geological models contain significant uncertainties (Wellmann et al., 2010; Bardossy and Fodor, 2004; Lark et al., 2013; Caers, 2011; McLane et al., 2008; Chatfield, 1995) that must be addressed thoughtfully to reach a plausible level of confidence in the model. However, treating geological modeling stochastically

715 implies many considerations: (i) from tens or hundreds of variables involved in the mathematical equations which ones should be latent?; (ii) can we filter all the possible outcomes which represent unreasonable geological settings? and (iii) how can we use other sources of data—especially geophysics—to improve the accuracy of the inference itself?

The answers to these questions are still actively debated in research and are highly dependent

720 on the type of mathematical and computational framework chosen. ~~In the interpolation method explained—Uncertainty quantification and its logical extension into probabilistic machine learning will not be covered in the depth~~ in this paper ~~the parameters suitable to behave as a latent variables (see figure 4 for an overview of possible stochastic parameters) could be the~~ due to the broad scope of the subject. However, the main goal of *GemPy* is to serve as main generative model within these

725 ~~probabilistic approaches and as such we will provide a demonstration of how *GemPy* fits on the workflow of our previous work (de la Varga and Wellmann, 2016; Wellmann et al., 2017) as well as how this work may set the foundations for an easier expansion into the domain of probabilistic machine learning in the future.~~

~~As we have seen so far, the CoKriging algorithm here enables the construction of geological~~

730 ~~models for a wide range of geometric and topological settings with a limited number of parameters (Figure 4 red):~~

- ~~– geometric parameters, interface points \mathbf{x}_α (i.e. the 3 Cartesian coordinates x, y, z), orientations—orientations \mathbf{x}_β (i.e. the 3 Cartesian coordinates x, y, z and the plane orientation normal Gx, Gy, Gz) or densities for the computation of the forward gravity. But not only parameters with physical meaning are suitable to be considered stochastic. Many mathematical parameters used in the kriging interpolation—such as:~~
 - ~~– geophysical parameters, e.g. density;~~
- 735

- model parameters, e.g. covariance at distance zero C_0 (i.e. nugget effect) or the range of the covariance r (see AppendixD for an example of a covariance function)—~~play a crucial role during the computation of the final models and, at best, are inferred by an educated guess to a greater or lesser extent (Chiles et al., 2004; Calcagno et al., 2008). To tackle this problem in a strict manner, it would be necessary to combine Bayesian statistics, information theory and sensitivity analysis among other expertises, but in essence all these methodologies begin with a probabilistic programming framework.~~

Therefore, an implicit geological model is simply a graphical representation of a deterministic mathematical operation of these parameters and as such, any of these parameters are suitable to behave as latent variables. From a probabilistic point of view *GemPy* would act as the generative model that links two or more data sets.

GemPy is fully designed to be coupled with probabilistic frameworks, in particular with *pymc3* (Salvatier et al., 2016) as both libraries are based on *Theano*.

pymc is a series of Python libraries that provide intuitive tools to build and subsequently infer complex probabilistic graphical models (~~see Koller and Friedman, 2009, and figure ?? as an example of a PGM~~)(see Koller and Friedman

These libraries offer expressive and clean syntax to write and use statistical distributions and different samplers. At the moment two main libraries coexist due to their different strengths and weaknesses.

On the one hand, we have *pymc2* (Patil et al., 2010) written in FORTRAN and Python. *pymc2* does not allow gradient based sampling methods, since it does not have automatic differentiation capabilities. However, for that same reason, the model construction and debugging is more accessible. Furthermore, not computing gradients enables an easy integration with 3rd party libraries and easy extensibility to other scientific libraries and languages. Therefore, for prototyping and lower dimensionality problems—where the posterior can be tracked by Metropolis-Hasting methods (Haario et al., 2001)—*pymc2* is still the go-to choice.

On the other hand the latest version, *pymc3* (Salvatier et al., 2016), allows the use of next generation gradient-based samplers such as No-U-Turn Sampler (Hoffman and Gelman, 2014) or Automatic Variational Inference (Kucukelbir et al., 2015). These sampling methods are proving to be a powerful tool to deal with multidimensional problems—i.e. models with high number of uncertain parameters (Betancourt et al., 2017). The weakness of these methods are that they rely on the computation of gradients, which in many cases cannot be manually derived. To circumvent this limitation *pymc3* makes use of the AD capabilities of *Theano*. Being built on top of *Theano* confer to the Bayesian inference process all the capabilities discussed in section 2.3.2 in exchange for the clarity and flexibility that pure Python provides.

In this context, the purpose of *GemPy* is to fill the gap of complex algebra between the prior data and observations, such as geophysical responses (e.g. gravity or seismic inversions) or geological interpretations (e.g. tectonics, model topologies). Since *GemPy* is built on top of *Theano* as well, the compatibility with both libraries is relatively straightforward. However, being able to

775 encode most of the conceivable probabilistic graphical models derived from, often, diverse and heterogeneous data would be an herculean task. For this reason most of the construction of the PGM has to be coded by the user using the building blocks that the *pymc* packages offer (see [listing 6](#)) (Bishop, 2013; Patil et al., 2010; Koller and Friedman, 2009, and see e.g. [listing 6](#)). By doing so, we can guarantee full flexibility and adaptability to the necessities of every individual geological setting.

780 For this paper we will use *pymc2* for its higher readability and simplicity. *pymc3* architecture is analogous with the major difference that the PGM is constructed in *Theano*—and therefore symbolically (for examples using *pymc3* and *GemPy* check the online documentation detailed in Appendix A2).

785 3.4.1 Uncertainty Quantification

An essential aspect of probabilistic programming is the inherent capability to quantify uncertainty. Monte Carlo error propagation (Ogilvie, 1984) has been introduced in the field of geological modeling a few years ago (Wellmann et al., 2010; Jessell et al., 2010; Lindsay et al., 2012), exploiting the automation of the model construction that implicit algorithms offer.

790 In this paper example (figure 9-Priors), we fit a normal distribution of standard deviation 300[m] around the Z axis of the interface points in initial model (figure 3 c). In other words, we allow to the interface points that define the model to oscillate independently along the axis Z accordingly randomly—using normal distributions—and subsequently we compute the geomodels that these new data describe. [The choice of perturbing only the Z axis is merely due to computational limitations.](#)

795 [Uncertainty tends to be higher in this direction \(e.g. wells data or seismic velocity\), however there is a lot of room for further research on the definition of prior data—i.e. its choice and probabilistic description—on both directions, to ensure that we properly explore the space of feasible models and to generate a parametric space as close as possible to the posterior.](#)

The first step to the creation of a PGM is to define the parameters that are supposed to be stochastic and the probability functions that describe them. To do so, *pymc2* provides a large selection of distributions as well as a clear framework to create custom ones. Once we created the stochastic parameters we need to substitute the initial value in the *GemPy* database (`interp_data` in the snippets) for the corresponding *pymc2* objects. Next, we just need to follow the usual *GemPy* construction process—i.e. calling the `compute_model` function—wrapping it using a deterministic

800 *pymc2* decorator to describe that these function is part of the probabilistic model (figure [??8](#)). After creating the graphical model we can sample from the stochastic parameters using Monte Carlo sampling using *pymc2* methods.

Listing 6. Probabilistic model construction and inference using *pymc2* and *GemPy*: Monte Carlo forward simulation (see figure 9-Priors for the results).

...

810 Add Listing 3

```

...

# Coping the initial data
geo_data_stoch_init = deepcopy(interp_data.geo_data_res)
815 # MODEL CONSTRUCTION
# =====
# Positions (rows) of the data we want to make stochastic
ids = range(2,12)

820 # List with the stochastic parameters. pymc.Normal attributes: Name, mean, std
interface_Z_modifier = [pymc.Normal("interface_Z_mod_"+str(i), 0., 1./0.01**2) for i in ids]

# Modifying the input data at each iteration
@pymc.deterministic(trace=True)
825 def input_data(\DIFdelbegin \DIFdel{value = 0, }\DIFdelend interface_Z_modifier =
    interface_Z_modifier,
    geo_data_stoch_init = geo_data_stoch_init,
    ids = ids, verbose=0):

830 # First we extract from our original interp_data object the numerical data that
# is necessary for the interpolation. geo_data_stoch is a pandas Dataframe
geo_data_stoch = gp.get_data(geo_data_stoch_init, numeric=True)

# Now we loop each id which share the same uncertainty variable. In this case, each layer. We
835 add the stochastic part to the initial value
    for num, i in enumerate(ids):
        interp_data.geo_data_res.interfaces.set_value(i, "Z",
            geo_data_stoch_init.interfaces.iloc[i]["Z"] + interface_Z_modifier[num])

840 # Return the input data to be input into the modeling function. Due to the way pymc2
# stores the traces we need to save the data as numpy arrays
    return interp_data.geo_data_res.interfaces[["X", "Y", "Z"]].values,
        interp_data.geo_data_res.orientations[["X", "Y", "Z", "dip", "azimuth",
            "polarity"]].values

845 # Computing the geological model
@pymc.deterministic(trace=True)
def gempy_model(value=0, input_data=input_data, verbose=False):

850 # modify input data values accordingly
    interp_data.geo_data_res.interfaces[["X", "Y", "Z"]] = input_data[0]

# Gx, Gy, Gz are just used for visualization. The Theano function gets azimuth dip and
polarity!!!
855    interp_data.geo_data_res.orientations[["G_x", "G_y", "G_z", "X", "Y", "Z", 'dip',
        'azimuth', 'polarity']] = input_data[1]

# Some iterations will give a singular matrix, that's why we need to
# create a try to not break the code.
860    try:
        lb, fb, grav = gp.compute_model(interp_data, outup='gravity')
        return lb, fb, grav

    except np.linalg.linalg.LinAlgError as err:
865 # If it fails (e.g. some input data combinations could lead to

```



```

# a singular matrix and thus break the chain) return an empty model
# with same dimensions (just zeros)
    if verbose:
        print("Exception_occured.")
870     return np.zeros_like(lith_block), np.zeros_like(fault_block), np.zeros_like(
        grav_i)

# Extract the vertices in every iteration by applying the marching cube algorithm
@pymc.deterministic(trace=True)
875 def gempy_surfaces(value=0, gempy_model=gempy_model):
    vert, simp = gp.get_surfaces(interp_data, gempy_model[0][1], gempy_model[1][1],
                                original_scale=True)

    return vert

880 # We add all the pymc objects to a list
params = [input_data, gempy_model, gempy_surfaces, *interface_Z_modifier]

# We create the pymc model i.e. the probabilistic graph
model = pymc.Model(params)
885 runner = pymc.MCMC(model)

# BAYESIAN INFERENCE
# =====
# Number of iterations
890 iterations = 10000

# Inference. By default without likelihoods: Sampling from priors
runner.sample(iter=iterations, verbose=1)

```

895 The suite of possible realization of the geological model are stored, as traces, in a database of choice (HDF5, SQL or Python pickles) for further analysis and visualization.

In 2-D we can display all possible locations of the interfaces on a cross-section at the center of the model (see figure 9-Priors-2-D representation), however the extension of uncertainty visualization to 3D is not as trivial. *GemPy* makes use of the latest developments in uncertainty visualization for 3-D structural geological modeling (e.g Lindsay et al., 2012, 2013a, b; Wellmann and Regenauer-Lieb, 2012). The first method consists on representing the probability of finding a given geological unit F at each discrete location in the model domain. This can be done by defining a probability function

$$p_F(x) = \sum_{k \in n} \frac{I_{F_k}(x)}{n} \quad (11)$$

where n is the number of realizations and $I_{F_k}(x)$ is a indicator function of the mentioned geological unit (figure 9-Probability shows the probability of finding Layer 1). However this approach can only display each unit individually. A way to encapsulate geomodel uncertainty with a single parameter to quantify and visualize it, is by applying the concept of information entropy [Wellmann and Regenauer-Lieb \(2012\)](#) ([Wellmann and Regenauer-Lieb, 2012](#)), based on the general concept developed by (Shannon, 1948). For a discretized geomodel the information entropy H (nor-

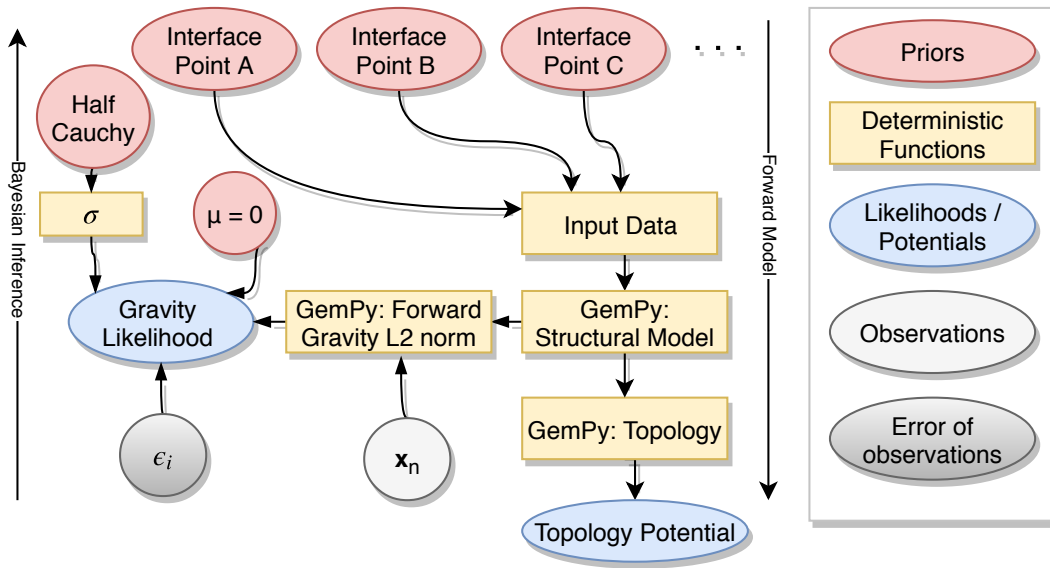


Figure 8. Probabilistic Programming results on a cross-section at the middle of the graphical model ($Y=10000[m]$) generated with pymc2. (i) Priors-UQ shows the uncertainty of geological models given Ellipses represent stochastic values to the Z position parameters, while rectangles are deterministic functions that return intermediated states of the input data ($\sigma=300$): (top) 2-D interface representation; (middle) probability of occurrence for Layer 1; (bottom) information entropy. (ii) Representation of data used as likelihood functions: (top) ideal topology graph; (middle) Synthetic probabilistic model taken such as reference for the gravity inversion; (bottom) Reference forward gravity overlain on top of an XY cross-section of the synthetic reference GemPy model. Posterior analysis after combining priors and likelihood in a Bayesian inference: (top) 2-D interface representation; (middle) probability of occurrence for Layer 1; (bottom) information entropy.

malized by the total number of voxels n) can be defined as

$$H = - \sum_{i=1}^n p_i \log_2 p_i \quad (12)$$

where p_i represents the probability of a layer at cell x . Therefore, we can use information entropy to compress our uncertainty reduce the dimensionality of probability fields into a single value at each voxel as an indication of uncertainty, reflecting the possible number of outcomes and their relative probability (see figure 9-Entropy).

3.4.2 Geological inversion: Gravity and Topology

Although computing the forward gravity has its own value for many applications, the main aim of GemPy is to integrate all possible sources of information into a single probabilistic framework. The use of likelihood functions in a Bayesian inference in opposition to simply rejection sampling comparison to simple forward simulation has been explored by the authors during the recent years

(de la Varga and Wellmann, 2016; Wellmann et al., 2017; Schaaf, 2017). This approach enables to tune the conditioning of possible stochastic realizations by varying the probabilistic density function used as likelihoods. In addition, Bayesian networks allow to combine several likelihood functions, generating a competition among the prior distribution of the input data and likelihood functions resulting in posterior distributions that best honor all the given information. To give a flavor of what is possible, we apply custom likelihoods to the previous example based on, topology and gravity constrains in an inversion.

As, we have shown above, topological graphs can represent the connectivity among the segmented areas of a geological model. As is expected, stochastic perturbations of the input data can rapidly alter the configuration of mentioned graphs. In order to preserve a given topological configuration partially or totally, we can construct specific likelihood functions. To exemplify the use of a topological likelihood function, we will use the topology computed in the section 3.3 derived from the initial model realization (figure 7 or 9-Likelihoods) as "ideal topology". This can be based on an expert interpretation of kinematic data or deduced from auxiliary data.

The first challenge is to find a metric that captures the similarity of two graphs. As a graph is nothing but a set of nodes and their edges we can compare the intersection and union of two different sets using the the Jaccard index (Jaccard, 1912; Thiele et al., 2016a). It calculates the ratio of intersection and union of two given graphs A and B:

$$J(A, B) = \frac{|A \cap B|}{|A \cup B|} \quad (13)$$

The resulting ratio is zero for entirely different graphs, while the metric rises as the sets of edges and nodes become more similar between two graphs and reaches exactly one for an identical match. Therefore, the Jaccard index can be used to express the similarity of topology graphs as a single number we can evaluate using a probability density function. ~~The type of probability density function used will determine the "strength" or likelihood that the mean graph represent. Here, To~~
~~evaluate the likelihood of the simulated model topology~~ we use a ~~half-Cauchy distribution ($\alpha=0$ and $\beta=10^{-3}$) due to its tolerance to outliers~~ factor potential with a half-Cauchy parametrization (rate parameter $\beta = 10^{-3}$) to constrain our model using the soft data of our topological knowledge (Lauritzen et al., 1990; Jordan, 1998; Christakos, 2002). This specific parametrization was chosen due to empirical evidence from different model runs to allow for effective parameter space exploration in the used MCMC scheme.

Listing 7. Probabilistic model construction and inference using *pymc2* and *GemPy*: Bayesian Inference (see figure 9 for the results).

```
...
Add Listing 6
...
# Computation of topology
@pymc.deterministic(trace=True)
```

```

def gempy_topo(value=0, gm=gempy_model, verbose=False):
    G, c, lu, lot1, lot2 = gp.topology_compute(gem_data, gm[0][0], gm[1], cell_number=0,
960         direction="y")

    if verbose:
        gp.plot_section(gem_data, gm[0][0], 0)
        gp.topology_plot(gem_data, G, c)
965

    return G, c, lu, lot1, lot2

# Computation of L2-Norm for the forward gravity
@pymc.deterministic
970 def e_sq(value = original_grav, model_grav = gempy_model[2], verbose = 0):
    square_error = np.sqrt(np.sum((value*10**-7 - (model_grav*10**-7))**2))
    return square_error

# Likelihoods
975 # =====
@pymc.stochastic
def like_topo_jaccard_cauchy(value=0, gempy_topo=gempy_topo, G=topo_G):
    """Compares the model output topology with a given topology graph G using an inverse Jaccard-
        index embedded in a half-cauchy likelihood."""
980 # jaccard-index comparison
        j = gp.Topology.compare_graphs(G, gempy_topo[0])
        # the last parameter adjusts the "strength" of the likelihood
        return pymc.half_cauchy_like(1 - j, 0, 0.001)

985 @pymc.observed
def inversion(value = 1, e_sq = e_sq):
    return pymc.half_cauchy_like(e_sq, 0, 0.1)

# We add all the pymc objects to a list
990 params = [input_data, gempy_model, gempy_surfaces, gempy_topo, *interface_Z_modifier,
    like_topo_jaccard_cauchy, e_sq, inversion]

# We create the pymc model i.e. the probabilistic graph
model = pymc.Model(params)
995 runner = pymc.MCMC(model)

# BAYESIAN INFERENCE
# =====
# Number of iterations
1000 iterations = 15000

# Inference. Adaptive Metropolis
runner.use_step_method(pymc.AdaptiveMetropolis, params, delay=1000)
1005 runner.sample(iter = 20000, burn=1000, thin=20, tune_interval=1000, tune_throughout=True)

```

Gravity likelihoods [aim to](#) exploit the spatial distribution of density which can be related to different lithotypes (Dentith and Mudge, 2014). To test the likelihood function based on gravity data, we first generate the synthetic "measured" data. This was done simply by computing the forward gravity for one of the extreme models (to highlight the effect that a gravity likelihood can have) generated during the Monte Carlo error propagation in the previous section. This model is particularly

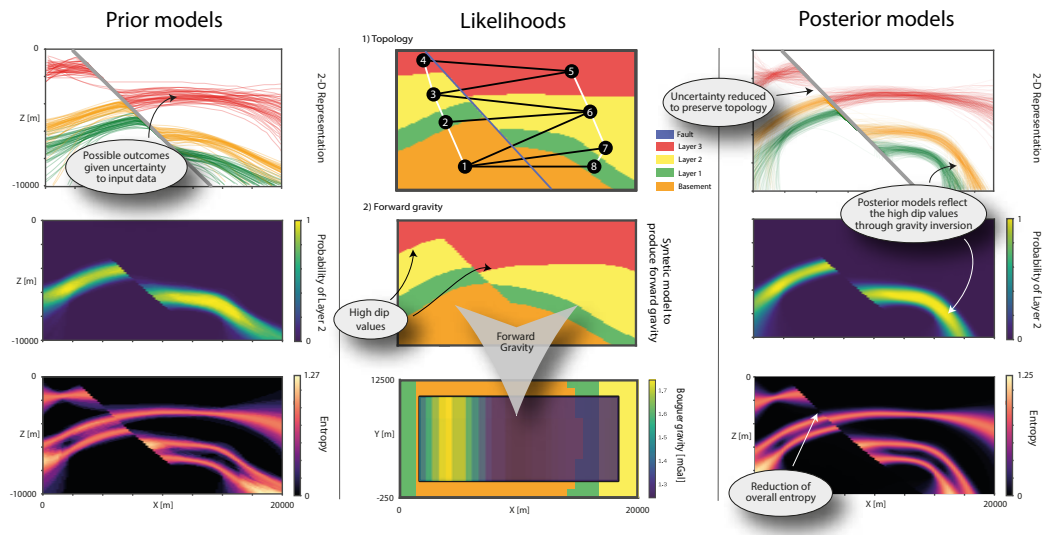


Figure 9. Probabilistic Programming results on a cross-section at the middle of the model ($Y = 10000 [m]$). (i) Priors-UQ shows the uncertainty of geological models given stochastic values to the Z position of the input data (standard deviation, $\sigma = 300$): (top) 2-D interface representation ; (middle) probability of occurrence for Layer 2; (bottom) information entropy. (ii) Representation of data used as likelihood functions: (top) ideal topology graph; (middle) Synthetic model taken as reference for the gravity inversion; (bottom) Reference forward gravity overlain on top of an XY cross-section of the synthetic reference model. Posterior analysis after combining priors and likelihood in a Bayesian inference: (top) 2-D interface representation; (middle) probability of occurrence for Layer 2; (bottom) information entropy.

characteristic by its high dip values (figure 9-Syntetic model to produce forward gravity). Once we have an "observed" gravity, we can compare it to a simulated gravity response. To do so, we compare their values. The construction of the likelihood function is done applying an L2-norm encapsulating the difference into a single error value. This error value acts as the input of the likelihood function; in this case, between each "measured" data point and the forward computation and evaluating the result by a normal distribution of mean $\mu = 0$ and with the standard deviation, σ as a half Cauchy ($\alpha = 0$ and $\beta = 10^{-1}$ prior (rate parameter $\beta = 10^{-1}$). This probabilistic density function increases as we approach to 0 and at both extremes (very low or high values of error) the function flattens to accommodate to possible measurement errors. The likelihood function will push the model parameters (figure 4, red) in the direction to reduce the L2-norm as much as possible while keeping the standard deviation around the prior value (this prior value encapsulate the inherent measurement and model uncertainty).

As sampler we use an adaptive Metropolis method. Defining the topology potential and gravity likelihood on the same Bayesian network creates a joint likelihood value that will define the posterior space. To sample from the posterior we use adaptive Metropolis (Haario et al., 2001, for a more in depth explanation of samplers and their importance see de la Varga and Wellmann, 2016). This

method varies the metropolis sampling size according to the covariance function that gets updated every n iterations. For the results here exposed, we performed 20000 iterations, tuning the adaptive covariance every 1000 steps (a convergence analysis can be found in the Jupyter notebooks attached to the on-line supplement of this paper).

As a result of applying likelihood functions we can appreciate a clear change in the posterior (i.e. the possible outcomes) of the inference. A closer look shows two main zones of influence, each of them related to one of the likelihood functions. On one hand, we observe a reduction of uncertainty along the fault plane due to the restrictions that the topology function imposes by conditioning the models to high Jaccard values. On the other hand, what in the first example—i.e. Monte Carlo error propagation—was propagation, left on Figure 9—was just an outlier, due to the influence of the gravity inversion, now it becomes the norm bending the layers pronouncedly. In both cases, it is important to keep in mind that the grade of impact into the final model is inversely proportional to the amount of uncertainty that each stochastic parameter carries. Finally, we would like to remind the reader that the goal of this example is not to obtain realistic geological models but to serve as an example how the in-built functionality of *GemPy* can be used to handle similar cases. The purpose of this example is to highlight the functionality. For a realistic study, further detailed adjustments would have to be taken

4 Discussion

We have introduced *GemPy*, a Python library for implicit geomodelling with special emphasis on the analysis of uncertainty. With the advent of powerful implicit methods to automate many of the geological modeling steps, *GemPy* builds on these mathematical foundations to offer a reliable and easy-to-use technology to generate complex models with only a few lines of code. In many cases—and in research in particular—it is essential to have transparent software that allows full manipulation and understanding of the logic beneath its front-end to honor the scientific method and allows reproducibility by open-access to it.

Up until now, implicit geological modeling was limited to proprietary software suites—for the petroleum industry (GoCad, Petrel, JewelSuite) or the mining sector (MicroMine, MIRA Geoscience, GeoModeller, Leapfrog)—with an important focus on industry needs and user experience (e.g. graphical user interfaces or data compatibilities). Despite the access to the APIs of many of these softwares, their lack of transparency and the inability to fully manipulate any of the algorithms represents a serious obstacle for conducting appropriate *reproducible* research. To overcome these limitations, many scientific communities—e.g. *simpeg* in geophysics (Cockett et al., 2015), *astropy* in astronomy (Robitaille et al., 2013) or *pynoddy* in kinematic structural modeling (Wellmann et al., 2016)—are moving towards the open-source frameworks necessary for the full application of the scientific method. In this regard, the advent of open-source programming languages such as R or

Python are playing a crucial role in facilitating scientific programming and enabling the crucial reproducibility of simulations and script-based science. *GemPy* aims to fill the existing gap of implicit modeling in the open-source ecosystem in geosciences ~~that until now had to be filled by expensive~~
1065 ~~general-purpose commercial softwares.~~

Implicit methods rely on interpolation functions to automate some or all the construction steps. Different mathematical approaches have been developed and improved in the recent years to tackle many of the challenges that particular geological settings pose (e.g. Lajaunie et al., 1997; Hillier et al., 2014; Calcagno et al., 2008; Caumon et al., 2013; Caumon, 2010). A significant advantage of
1070 some of these methods is that they directly enable the re-computation of the entire structure when input data is changed or added. Furthermore, they can provide a geological meaningful interpolation function, for example considering deposition time (Caumon, 2010) or potential-fields (Lajaunie et al., 1997) to encapsulate the essence of geological deposition in different environments. The creation of *GemPy* has been made possible in a moment when the automation of geological modeling
1075 via implicit algorithms, as well as the maturity of the Python open-source ecosystem reached a point where a few thousand new lines of code are able to perform efficiently the millions of linear algebra operations and complex memory management necessary to create complex geological models. An important aspect in *GemPy*'s design has been the willingness to allow users to simply use *GemPy* as a tool to construct geological models for different purposes as well as to encourage users to develop
1080 and expand ~~*GemPy*'s~~ the code base itself. With the purpose to facilitate a low entry barrier we have taken two main structural decisions: (i) a clear separation between core features and extensible assets and (ii) combination of functional and object-oriented programming. The aim of this dual design is to give a friendly, easy-to-use front-end to the majority of users while keeping a modular structure of the code for future contributors.

Using *GemPy* requires a minimum familiarity with the Python syntax. The lack of an advanced graphical interface to place the input data interactively forces the user to provide data sets with the coordinates and angular data. For this reason, for complex initial models *GemPy* could be seen more as a back-end library required to couple it with software providing 3-D graphical manipulation. Due to the development team's background, *GemPy* is fully integrated with GeoModeller through
1090 the built-in library *pygeomod*. *GemPy* is able to read and modify GeoModeller projects directly, allowing to take advantage of their respective unique features. All input data of *GemPy* itself is kept in open, standard Python formats, making use of the flexible *pandas* DataFrames and powerful *numpy* arrays. Hence, every user will be able to freely manipulate the data at any given point.

GemPy has built-in functionality to visualize results using the main visualization libraries offered
1095 in Python: *matplotlib* for 2-D and *vtk* for 3-D and allows to export `.vtk` files for later visualization in common open-source tools for scientific visualizations such as ParaView. ~~Altought~~ Although *GemPy* does not include an evolved user interface, we offer certain level of interactivity using *GemPy*'s build-in 3-D visualization in *vtk* and interactive data frames through *qgrid*. Not only is the user able

to move the input data via drag-and-drop [or changing the data frame](#), but *GemPy* can immediately re-
1100 interpolate the perturbed model, enabling an extremely intuitive direct feedback on how the changes
made affect the model. Visualization of vast model ensembles is also possible in 3-D using slider
functionality. Future plans for the visualization of *GemPy* include virtual reality support to make
data manipulation and model visualization more immersive and intuitive to use.

Another important feature of *GemPy* is the use of symbolic code. The lack of domain specific
1105 language allows the compilation of the code to a highly efficient language. Furthermore, since all
the logic has to be described prior to the compilation, memory allocation and parallelization of the
code can be optimized. *Theano* uses BLAS (Lawson et al., 1979) to perform the algebraic operations
with out of the box Open MP (Dagum and Menon, 1998) capabilities for multi-core operations.
Additionally, parallel GPU computation is available and compatible with the use of CPUs, which
1110 allows to define certain operations to a specific device and even to split big arrays (e.g. grid) to
multiple GPUs. In other words, the symbolic nature of the code enables the separation of the logic
according to the individual advantages of each device—i.e. sequential computations to CPUs and
parallel calculations to the GPUs—allowing for better use of the available hardware. Hence, this
scheme is portable to high performance computing in the same fashion.

1115 Up to [today now](#), structural geological models have relied significantly on the best deterministic,
explicit realization that an expert is ~~capable to create~~ [able to construct](#) using often noisy and sparse
data. Research into the interpretation uncertainty of geological data sets (e.g. seismic data) has recog-
nized the significant impact of interpreter education and bias on the extracted input data for geolog-
ical models (e.g. Bond et al., 2007; Bond, 2015). *GemPy*'s ability to be enveloped into probabilistic
1120 programming frameworks such as *pymc*, allows for the consideration of input data uncertainties and
could provide a free, open-source foundation for developing probabilistic geomodeling workflows
which integrate uncertainties from the very beginning of data interpretation, through the geomodel
interpolation up to the geomodel application (e.g. flow simulations, economic estimations).

In the transition to a world dominated by data and optimization algorithms—e.g. deep neural
1125 networks or big data analytics—there are many attempts to apply those advances in geological mod-
eling (Wang et al., 2017; Gonçalves et al., 2017). The biggest attempt to use data driven models
in geology comes from geophysical inversions (Tarantola and Valette, 1982; Mosegaard and Taran-
tola, 1995; Sambridge and Mosegaard, 2002; Tarantola, 2005). Their approaches consist of using
the mismatch of one or many parameters, comparing model with reality, modifying them accord-
1130 ingly until reaching a given tolerance. However, since this solution is never unique, it is necessary
to enclose the space of possibilities by some other means. This prior approach to the final solution
usually is made using polygonal or elliptic bodies leading to oversimplified geometry of the distinct
lithological units. Other researchers use the additional data—geophysical data or other constrains
(Jessell et al., 2010; Wellmann et al., 2014)— to validate multiple possible realizations of geological
1135 models generated either automatically by an interpolation function or manually. Here, the additional

information is used as a hard deterministic filter of what is reasonable or not. The limitation of pure rejection filtering is that information does not propagate backward to modify the latent parameters that characterize the geological models what makes computational infeasible to explore high dimensional problems. In between these two approaches, we can find some attempts to reconcile both approaches meeting somewhere in the middle. An example of this is the approach followed in the software packages GeoModeller and SKUA. They optimize the layer densities, and when necessary the discretized model, to fit the geological model to the observed geophysical response. The consequence of only altering the discrete final model is that after optimization the original input data used for the construction of the geological model (i.e. interface points and orientation data) gets overwritten and consequently hard to reproduce.

We propose a more ~~global~~general approach. By embedding the geological model construction into a ~~model-based~~probabilistic machine learning framework (Bishop, 2013)—i.e. a Bayesian inference network. In short a Bayesian inference is a mathematical formulation to update beliefs in the light of new evidence. This statement applied to geological modeling is translated into keeping all or a subset of the parameters that generate the model uncertain and evaluate the quality of the model comparing its mismatch with additional data or geological knowledge encoded mathematically (de la Varga and Wellmann, 2016). In this way, we are able to utilize available information not only in a forward direction to construct models, but also propagate information backwards in an inverse scheme to refine the probabilistic distributions that characterize the modeling parameters. Compared with previous approaches, we do not only use the inversion to improve a deterministic model but instead to learn about the parameters that define the model to begin with. In recent years, we have shown how this approach may help closing the gap between geophysical inversions and geological modeling in an intuitive manner (Wellmann et al., 2017). At the end of the day, Bayesian inferences operate in a very similar way to how humans do: we create our best guess model; we compare it to the geophysical data or our geological knowledge and in case of disagreement we modify the input of the geological model in the direction we think is the best to honor the additional data.

Despite the convincing mathematical formulation of Bayesian inferences, there are caveats to be dealt with for practical applications. As mentioned in Section 3.4, the effective computational cost to perform such algorithms have prohibited its use beyond research and simplified models. However, recent developments in MCMC methods enable more efficient ways to explore the parametric space and hence opening the door to a significant increase on the complexity of geological models. An in-depth study of the impact of gradient-based MCMC methods in geological modeling will be carried out in a future publication.

Nevertheless, performing AD does not come free of cost. The required code structures limit the use of libraries which do not perform AD themselves, which in essence imposes to rewrite most of the mathematical algorithms involved in the Bayesian network. Under these circumstances, we have rewritten in *Theano* the potential field method—with many of the add-ons developed in recent years

(Calcagno et al., 2008)—and the computation of forward gravity responses for discrete rectangular prisms.

1175 Currently *GemPy* is in active development moving towards three core topics: (i) increasing the ~~model-based~~-probabilistic machine learning capabilities by exploiting gradient based methods and new types of likelihoods; (ii) post-processing of uncertainty quantification and its relation to decision theory and information theory; and (iii) exploring the new catalog of virtual reality and augmented reality solutions to improve the visualization of both the final geological models and the
1180 building environment. ~~However, ideally~~ Ideally *GemPy* will function as a platform to create a vibrant open-source community to push forward geological modeling into the new machine learning era. Therefore, we hope to include functionality developed by other external users into the main package.

In conclusion, *GemPy* has evolved to a full approach for geological modelling in a probabilistic
1185 programming framework. The lack of available open-source tools in geological modeling and the necessity of writing all the logic symbolically has pushed the project to an unexpected stand-alone size. However, this would not have been possible without the immense, ever-growing open-source community which provide numerous and high-quality libraries that enable the creation of powerful software with relative few new lines of code. And in the same fashion, we hope the community will
1190 make use of our library to perform geological modeling transparently, reproducibly and incorporating the uncertainties inherent to earth sciences.

Code availability

GemPy is a free, open-source Python library licensed under the GNU Lesser General Public License v3.0 (GPLv3). It is hosted on the GitHub repository <https://github.com/cgre-aachen/gempy> (DOI:
1195 10.5281/zenodo.1186118).

Appendix A: *GemPy* package information

A1 Installation

Installing *GemPy* can be done in two ways: (i) Either by cloning the GitHub repository with `$ git clone https://github.com/cgre-aachen/gempy.git` and then manually installing it
1200 by running the Python setup script in the repository: `$ python install.py` (ii) Or by using the Python Package Index (PyPI) with the command `$ pip install gempy`, which directly downloads and installs the library.

A2 Documentation

GemPy's documentaion is hosted on <http://gempy.readthedocs.io/>, which provides a
1205 general overview over the library and multiple in-depth tutorials. The tutorials are provided as
Jupyter Notebooks, which provide the the convenient combination of documentation and executable
script blocks in one document. The notebooks are part of the repository and located in the tutori-
als folder. See <http://jupyter.org/> for more information on installing and running Jupyter
Notebooks.

1210 A3 Jupyter notebooks

We provide Jupyter notebooks as part of the online documentation. These notebooks can be ex-
ecuted in a local Python environment (if the required dependencies are correctly installed, see
above). In addition, static versions of the notebooks can currently be inspected directly on the
github repository web page or through the use of nbviewer. In addition, it is possible to run in-
1215 teractive notebooks through the use of binder (provided through <https://mybinder.org> at the time
of writing). For more details and up-to-date information, please refer to the repository page <https://github.com/cgre-aachen/gempy>.

A4 Unit Tests

The *GemPy* package contains a set of tests, which can be executed in the standard Python testing
1220 environment. If you cloned or downloaded the repository, then these tests can directly be performed
by going to the package folder and run the pytest command: `$ pytest`

If all tests are successful, you are ready to continue.

Appendix B: Kriging system expansion

The following equations have been derived from the work in Aug (2004); Lajaunie et al. (1997);
1225 Chiles and Delfiner (2009).

B1 Gradient Covariance-Matrix $C_{\partial \mathbf{Z} / \partial \mathbf{u}}$

The gradient covariance-matrix, $C_{\partial \mathbf{Z} / \partial \mathbf{u}}$, is made up of as many variables as gradient directions that
are taken into consideration. In 3-D, we would have the Cartesian coordinates dimensions— $\mathbf{Z} / \partial x$,
 $\mathbf{Z} / \partial y$, and $\mathbf{Z} / \partial z$ —and therefore, they will derive from the partial differentiation of the covariance
1230 function $\sigma(x_i, x_j)$ of \mathbf{Z} .

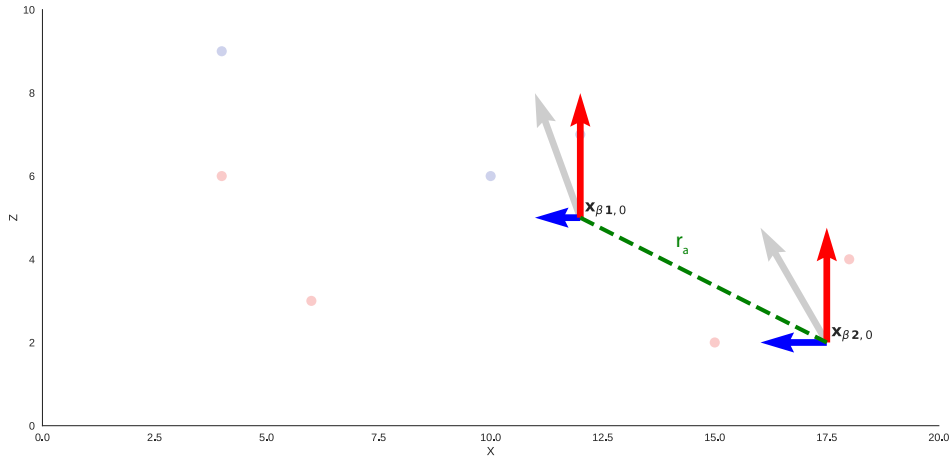


Figure 10. 2-D representation of the decomposition of the orientation vectors into Cartesian axis. Each Cartesian axis represent a variable of a sub CoKriging system. The dotted green line represent the covariance distance, r_a for the covariance of the gradient.

As in our case the directional derivatives used are the 3 Cartesian directions we can rewrite gradients covariance, $C_{\partial \mathbf{Z} / \partial \mathbf{u}, \partial \mathbf{Z} / \partial \mathbf{v}}$ for our specific case as:

$$C_{\partial \mathbf{Z} / \partial \mathbf{x}, \partial \mathbf{Z} / \partial \mathbf{y}, \partial \mathbf{Z} / \partial \mathbf{z}} = \begin{bmatrix} C_{\partial \mathbf{Z} / \partial \mathbf{x}, \partial \mathbf{Z} / \partial \mathbf{x}} & C_{\partial \mathbf{Z} / \partial \mathbf{x}, \partial \mathbf{Z} / \partial \mathbf{y}} & C_{\partial \mathbf{Z} / \partial \mathbf{x}, \partial \mathbf{Z} / \partial \mathbf{z}} \\ C_{\partial \mathbf{Z} / \partial \mathbf{y}, \partial \mathbf{Z} / \partial \mathbf{x}} & C_{\partial \mathbf{Z} / \partial \mathbf{y}, \partial \mathbf{Z} / \partial \mathbf{y}} & C_{\partial \mathbf{Z} / \partial \mathbf{y}, \partial \mathbf{Z} / \partial \mathbf{z}} \\ C_{\partial \mathbf{Z} / \partial \mathbf{z}, \partial \mathbf{Z} / \partial \mathbf{x}} & C_{\partial \mathbf{Z} / \partial \mathbf{z}, \partial \mathbf{Z} / \partial \mathbf{y}} & C_{\partial \mathbf{Z} / \partial \mathbf{z}, \partial \mathbf{Z} / \partial \mathbf{z}} \end{bmatrix} \quad (\text{B1})$$

1235 Notice, however, that covariance functions by definition are described in a polar coordinate system, and therefore it will be necessary to apply the chain rule for *directional derivatives*. Considering an isotropic and stationary covariance we can express the covariance function as:

$$\sigma(x_i, x_j) = C(r) \quad (\text{B2})$$

with:

$$r = \sqrt{h_x^2 + h_y^2} \sqrt{h_x^2 + h_y^2 + h_z^2} \quad (\text{B3})$$

1240 ~~therefore we need to apply the chain rule in partial differentiation. For the case of the covariance in a single direction :~~ and h_u as the distance $u_i - u_j$ in the given direction (usually Cartesian directions). Therefore, since we aim to derive $C_Z(r)$ respect an arbitrary direction u we must apply the *directional derivative* rules as follows:

$$C_{\partial \mathbf{Z} / \partial \mathbf{u}, \partial \mathbf{Z} / \partial \mathbf{u}} = \frac{\partial^2 C_Z(r)}{\partial h_u^2} = \frac{\partial C_Z(r)}{\partial r} \frac{\partial}{\partial h_u} \left(\frac{\partial r}{\partial h_u} \right) + \frac{\partial}{\partial h_u} \left(\frac{\partial C_Z(r)}{\partial r} \right) \frac{\partial r}{\partial h_u} \quad (\text{B4})$$

1245 where:

$$\frac{\partial C_Z(r)}{\partial r} = \frac{\partial C_Z(r)}{\partial r} = C'_Z(r) \quad (\text{B5})$$

$$\frac{\partial r}{\partial h_u} = \frac{h_u}{\sqrt{h_u^2 + h_v^2}} = -\frac{h_u}{r} \quad (\text{B6})$$

$$\frac{\partial}{\partial h_u} \left(\frac{\partial r}{\partial h_u} \right) = \frac{\partial}{\partial h_u} \left(\frac{h_u}{\sqrt{h_u^2 + h_v^2}} \right) = -\frac{2h_u^2}{2\sqrt{h_u^2 + h_v^2}} + \frac{1}{\sqrt{h_u^2 + h_v^2}} = -\frac{h_u^2}{r^3} + \frac{1}{r} \quad (\text{B7})$$

$$\frac{\partial}{\partial h_u} \left(\frac{\partial C_Z(r)}{\partial r} \right) = \frac{\partial C'_Z(r)}{\partial h_u} = \frac{\partial C'_Z(r)}{\partial r} \frac{\partial r}{\partial h_u} = -\frac{h_u}{r} C''_Z \quad (\text{B8})$$

1250 Substituting:

$$\mathbf{C}_{\partial \mathbf{Z} / \partial \mathbf{u}, \partial \mathbf{Z} / \partial \mathbf{u}} = C'_Z(r) \left(-\frac{h_u^2}{r^3} + \frac{1}{r} \right) - \frac{h_u}{r} C''_Z \frac{h_u}{r} = C'_Z(r) \left(-\frac{h_u^2}{r^3} + \frac{1}{r} \right) + \frac{h_u^2}{r^2} C''_Z \quad (\text{B9})$$

While in case of two different directions the covariance will be:

$$\mathbf{C}_{\partial \mathbf{Z} / \partial \mathbf{u}, \partial \mathbf{Z} / \partial \mathbf{v}} = \frac{\partial^2 C_Z(r)}{\partial h_u \partial h_v} = \frac{\partial C_Z(r)}{\partial r} \frac{\partial}{\partial h_v} \left(\frac{\partial r}{\partial h_u} \right) + \frac{\partial}{\partial h_v} \left(\frac{\partial C_Z(r)}{\partial r} \right) \frac{\partial r}{\partial h_u} \quad (\text{B10})$$

with:

$$1255 \quad \frac{\partial}{\partial h_v} \left(\frac{\partial r}{\partial h_u} \right) = \frac{\partial}{\partial h_v} \left(\frac{h_u}{\sqrt{h_u^2 + h_v^2}} \right) = -\frac{h_u h_v}{r^3} \quad (\text{B11})$$

$$\frac{\partial}{\partial h_v} \left(\frac{\partial C_Z(r)}{\partial r} \right) = \frac{\partial C'_Z(r)}{\partial h_v} = -C''_Z(r) \frac{h_v}{r} \quad (\text{B12})$$

we have:

$$\mathbf{C}_{\partial \mathbf{Z} / \partial \mathbf{u}, \partial \mathbf{Z} / \partial \mathbf{v}} = C'_Z(r) \left(-\frac{h_u h_v}{r^3} \right) + C''_Z(r) \frac{h_u h_v}{r^2} = \frac{h_u h_v}{r^2} \left(C''_Z(r) - \frac{C'_Z(r)}{r} \right) \quad (\text{B13})$$

This derivation is independent to the covariance function ~~choice, however~~ of choice. However, some

1260 covariances may lead to mathematical indeterminations if they are not sufficiently differentiable.

B2 Interface Covariance-Matrix

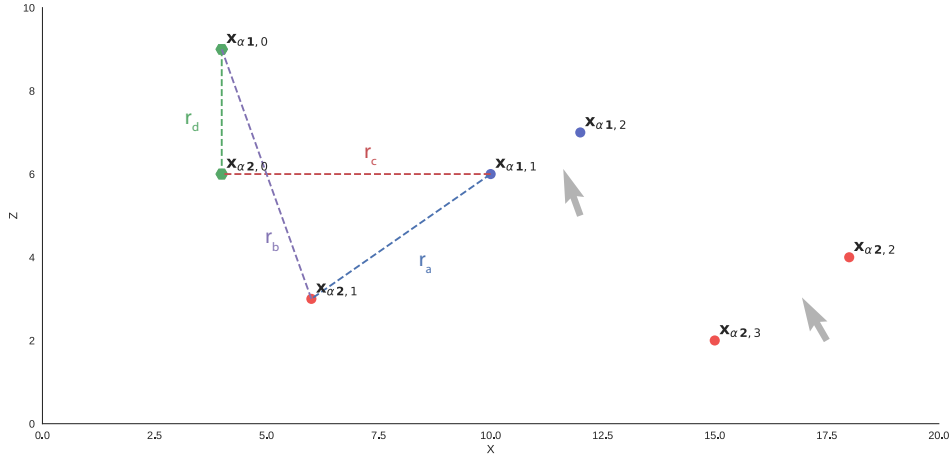


Figure 11. Distances r involved in the computation of the interface subsystem of the interpolation. Because all covariances are relative to a reference point $x_{\alpha,0}^i$, all four covariances with their respective distances, r_a, r_b, r_c and r_d must be taken into account (equation B14)

In a practical sense, keeping the value of the scalar field at every interface unfixed forces us to consider the covariance between the points within an interface as well as the covariance between different layers following equation,

$$C_{\mathbf{x}_{\alpha,i}^r, \mathbf{x}_{\alpha,j}^s} = \underbrace{C_{x_{\alpha,i}^r, x_{\alpha,j}^s}}_{r_a} - \underbrace{C_{x_{\alpha,0}^r, x_{\alpha,j}^s}}_{r_b} - \underbrace{C_{x_{\alpha,i}^r, x_{\alpha,0}^s}}_{r_c} + \underbrace{C_{x_{\alpha,0}^r, x_{\alpha,0}^s}}_{r_d} \quad (B14)$$

This lead to the subdivision of the CoKriging system respecting the interfaces:

$$C_{\mathbf{Z}, \mathbf{Z}} = \begin{bmatrix} C_{\mathbf{x}_{\alpha}^1, \mathbf{x}_{\alpha}^1} & C_{\mathbf{x}_{\alpha}^1, \mathbf{x}_{\alpha}^2} & \cdots & C_{\mathbf{x}_{\alpha}^1, \mathbf{x}_{\alpha}^s} \\ C_{\mathbf{x}_{\alpha}^2, \mathbf{x}_{\alpha}^1} & C_{\mathbf{x}_{\alpha}^2, \mathbf{x}_{\alpha}^2} & \cdots & C_{\mathbf{x}_{\alpha}^2, \mathbf{x}_{\alpha}^s} \\ \vdots & \vdots & \ddots & \vdots \\ C_{\mathbf{x}_{\alpha}^r, \mathbf{x}_{\alpha}^1} & C_{\mathbf{x}_{\alpha}^r, \mathbf{x}_{\alpha}^2} & \cdots & C_{\mathbf{x}_{\alpha}^r, \mathbf{x}_{\alpha}^s} \end{bmatrix} \quad (B15)$$

Combining Eq 5 and Eq B15 the covariance for the property potential-scalar field will look like:

$$C_{\mathbf{x}_{\alpha}^r, \mathbf{x}_{\alpha}^s} = \begin{bmatrix} C_{x_1^1 x_1^1} - C_{x_0^1 x_1^1} - C_{x_1^1 x_0^1} + C_{x_0^1 x_0^1} & C_{x_1^1 x_2^1} - C_{x_0^1 x_2^1} - C_{x_1^1 x_0^1} + C_{x_0^1 x_0^1} & \cdots & C_{x_1^1 x_j^1} - C_{x_0^1 x_j^1} - C_{x_1^1 x_0^1} + C_{x_0^1 x_0^1} \\ C_{x_2^1 x_1^1} - C_{x_0^1 x_1^1} - C_{x_2^1 x_0^1} + C_{x_0^1 x_0^1} & C_{x_2^1 x_2^1} - C_{x_0^1 x_2^1} - C_{x_2^1 x_0^1} + C_{x_0^1 x_0^1} & \cdots & C_{x_2^1 x_j^1} - C_{x_0^1 x_j^1} - C_{x_2^1 x_0^1} + C_{x_0^1 x_0^1} \\ \vdots & \vdots & \ddots & \vdots \\ C_{x_i^r x_1^s} - C_{x_0^r x_1^s} - C_{x_i^r x_0^s} + C_{x_0^r x_0^s} & C_{x_i^r x_2^s} - C_{x_0^r x_2^s} - C_{x_i^r x_0^s} + C_{x_0^r x_0^s} & \cdots & C_{x_i^r x_j^s} - C_{x_0^r x_j^s} - C_{x_i^r x_0^s} + C_{x_0^r x_0^s} \end{bmatrix} \quad (B16)$$

1270 B3 Cross-Covariance

In a CoKriging system, the relation between the interpolated parameters is given by a cross-covariance function. As we saw above, the gradient covariance is subdivided into covariances with respect to the three Cartesian directions (Eq B1), while the interface covariance is detached from the covariances matrices with respect to each individual interface (Eq B15). In the same manner, the cross-covariance
 1275 will reflect the relation of every interface to each gradient direction,

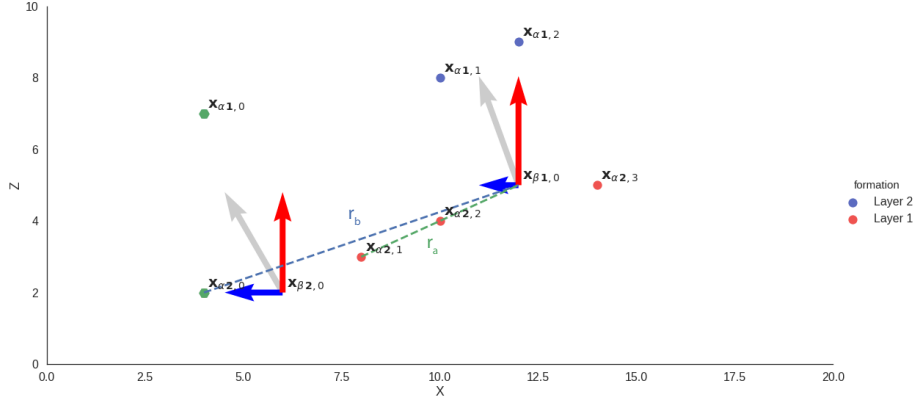


Figure 12. Distances r_a and r_b involved in the computation of the cross-covariance function. In a similar fashion as before, all interface covariance are computed relative to a reference point in each layer $x_{\alpha,0}^i$

$$C_{Z, \partial Z / \partial \mathbf{u}} = \begin{bmatrix} C_{\mathbf{x}_{\alpha 1}^1, \partial Z(\mathbf{x}_{\beta 1}) / \partial x} & C_{\mathbf{x}_{\alpha 2}^1, \partial Z(\mathbf{x}_{\beta 1}) / \partial x} & \cdots & C_{\mathbf{x}_{\alpha i}^r, \partial Z(\mathbf{x}_{\beta 1}) / \partial x} \\ C_{\mathbf{x}_{\alpha 1}^1, \partial Z(\mathbf{x}_{\beta 2}) / \partial x} & C_{\mathbf{x}_{\alpha 2}^1, \partial Z(\mathbf{x}_{\beta 2}) / \partial x} & \cdots & C_{\mathbf{x}_{\alpha i}^r, \partial Z(\mathbf{x}_{\beta 2}) / \partial x} \\ \vdots & \vdots & \ddots & \vdots \\ C_{\mathbf{x}_{\alpha 1}^1, \partial Z(\mathbf{x}_{\beta 1}) / \partial y} & C_{\mathbf{x}_{\alpha 2}^1, \partial Z(\mathbf{x}_{\beta 1}) / \partial y} & \cdots & C_{\mathbf{x}_{\alpha i}^r, \partial Z(\mathbf{x}_{\beta 1}) / \partial y} \\ C_{\mathbf{x}_{\alpha 1}^1, \partial Z(\mathbf{x}_{\beta 2}) / \partial y} & C_{\mathbf{x}_{\alpha 2}^1, \partial Z(\mathbf{x}_{\beta 2}) / \partial y} & \cdots & C_{\mathbf{x}_{\alpha i}^r, \partial Z(\mathbf{x}_{\beta 2}) / \partial y} \\ \vdots & \vdots & \ddots & \vdots \\ C_{\mathbf{x}_{\alpha 1}^1, \partial Z(\mathbf{x}_{\beta j-1}) / \partial z} & C_{\mathbf{x}_{\alpha 2}^1, \partial Z(\mathbf{x}_{\beta j-1}) / \partial z} & \cdots & C_{\mathbf{x}_{\alpha i}^r, \partial Z(\mathbf{x}_{\beta j-1}) / \partial z} \\ C_{\mathbf{x}_{\alpha 1}^1, \partial Z(\mathbf{x}_{\beta j}) / \partial z} & C_{\mathbf{x}_{\alpha 2}^1, \partial Z(\mathbf{x}_{\beta j}) / \partial z} & \cdots & C_{\mathbf{x}_{\alpha i}^r, \partial Z(\mathbf{x}_{\beta j}) / \partial z} \end{bmatrix} \quad (B17)$$

As the interfaces are relative to a point-reference point per later $\mathbf{x}_{\alpha 0}^k$ the value of the covariance function will be the difference between this point and the rest on the same layer:

$$C_{\mathbf{x}_{\alpha i}^r, \partial Z(\mathbf{x}_{\beta j}) / \partial x} = \underbrace{C_{Z(\mathbf{x}_{\alpha i}^r), \partial Z(\mathbf{x}_{\alpha j}) / \partial x}}_{r_a} \underbrace{C_{Z(\mathbf{x}_{\alpha i}^r), \partial Z(\mathbf{x}_{\beta j}) / \partial x}}_{r_b} \quad (B18)$$

1280 with the covariance of the scalar field being function the vector \mathbf{r} , its directional derivative is analogous to the previous derivations:

$$C_{Z, \partial Z / \partial \mathbf{u}} = \frac{\partial C_Z(r)}{\partial r} \frac{\partial r}{\partial h_u} = -\frac{h_u}{r} C'_Z \quad (B19)$$

B4 Universal matrix

As the mean value of the scalar field is going to be always unknown, it needs to be estimated from
 1285 data itself. The simplest approach is to consider the mean constant for the whole domain, i.e. ordinary
 Kriging. However, in the *scalar field* case we can assume certain drift towards the direction of the
 orientations. Therefore, the mean can be written as function of known basis functions:

$$\mu(\mathbf{x}) = \sum_{l=0}^L a_l f^l(\mathbf{x}) \quad (\text{B20})$$

where l is the grade of the polynomials used to describe the drift. Because of the algebraic depen-
 1290 dence of the variables, there is only one drift and therefore the unbiasedness can be expressed as:

$$\mathbf{U}_Z \lambda_1 + \mathbf{U}_{\partial \mathbf{Z} / \partial \mathbf{u}} \lambda_2 = f_{10} \quad (\text{B21})$$

Consequently, the number of equations are determined according to the grade of the polynomial and
 the number of equations forming the properties matrices equations B15 and B1:

$$U_Z = \begin{bmatrix} x_1^1 - x_0^1 & x_2^1 - x_0^1 & \dots & x_1^2 - x_0^2 & x_2^2 - x_0^2 & \dots & x_{i-1}^r - x_0^r & x_i^r - x_0^r \\ y_1^1 - y_0^1 & y_2^1 - y_0^1 & \dots & y_1^2 - y_0^2 & y_2^2 - y_0^2 & \dots & y_{i-1}^r - y_0^r & y_i^r - y_0^r \\ z_1^1 - z_0^1 & z_2^1 - z_0^1 & \dots & z_1^2 - z_0^2 & z_2^2 - z_0^2 & \dots & z_{i-1}^r - z_0^r & z_i^r - z_0^r \\ x_1^1 x_1^1 - x_0^1 x_0^1 & x_2^1 x_2^1 - x_0^1 x_0^1 & \dots & x_1^2 x_1^2 - x_0^2 x_0^2 & x_2^2 x_2^2 - x_0^2 x_0^2 & \dots & x_{i-1}^r x_{i-1}^r - x_0^r x_0^r & x_i^r x_i^r - x_0^r x_0^r \\ y_1^1 y_1^1 - y_0^1 y_0^1 & y_2^1 y_2^1 - y_0^1 y_0^1 & \dots & y_1^2 y_1^2 - y_0^2 y_0^2 & y_2^2 y_2^2 - y_0^2 y_0^2 & \dots & y_{i-1}^r y_{i-1}^r - y_0^r y_0^r & y_i^r y_i^r - y_0^r y_0^r \\ z_1^1 z_1^1 - z_0^1 z_0^1 & z_2^1 z_2^1 - z_0^1 z_0^1 & \dots & z_1^2 z_1^2 - z_0^2 z_0^2 & z_2^2 z_2^2 - z_0^2 z_0^2 & \dots & z_{i-1}^r z_{i-1}^r - z_0^r z_0^r & z_i^r z_i^r - z_0^r z_0^r \\ x_1^1 y_1^1 - x_0^1 y_0^1 & x_2^1 y_2^1 - x_0^1 y_0^1 & \dots & x_1^2 y_1^2 - x_0^2 y_0^2 & x_2^2 y_2^2 - x_0^2 y_0^2 & \dots & x_{i-1}^r y_{i-1}^r - x_0^r y_0^r & x_i^r y_i^r - x_0^r y_0^r \\ x_1^1 z_1^1 - x_0^1 z_0^1 & x_2^1 z_2^1 - x_0^1 z_0^1 & \dots & x_1^2 z_1^2 - x_0^2 z_0^2 & x_2^2 z_2^2 - x_0^2 z_0^2 & \dots & x_{i-1}^r z_{i-1}^r - x_0^r z_0^r & x_i^r z_i^r - x_0^r z_0^r \\ y_1^1 z_1^1 - y_0^1 z_0^1 & y_2^1 z_2^1 - y_0^1 z_0^1 & \dots & y_1^2 z_1^2 - y_0^2 z_0^2 & y_2^2 z_2^2 - y_0^2 z_0^2 & \dots & y_{i-1}^r z_{i-1}^r - y_0^r z_0^r & y_i^r z_i^r - y_0^r z_0^r \end{bmatrix} \quad (\text{B22})$$

$$\mathbf{U}_{\partial \mathbf{Z} / \partial \mathbf{u}} = \begin{bmatrix} \mathbf{x}_{\beta 1} & \mathbf{x}_{\beta 2} & \dots & \mathbf{x}_{\beta 1} & \mathbf{x}_{\beta 2} & \dots & \mathbf{x}_{\beta i-1} & \mathbf{x}_{\beta i} \\ 1 & 1 & \dots & 0 & 0 & \dots & 0 & 0 \\ 0 & 0 & \dots & 1 & 1 & \dots & 0 & 0 \\ 0 & 0 & \dots & 0 & 0 & \dots & 1 & 1 \\ 2x_1 & 2x_2 & \dots & 0 & 0 & \dots & 0 & 0 \\ 0 & 0 & \dots & 2y_1 & 2y_2 & \dots & 0 & 0 \\ 0 & 0 & \dots & 0 & 0 & \dots & 2z_{i-1} & 2z_i \\ y_1 & y_2 & \dots & x_1 & x_2 & \dots & 0 & 0 \\ y_1 & y_2 & \dots & 0 & 0 & \dots & x_{i-1} & x_i \\ 0 & 0 & \dots & z_1 & z_2 & \dots & x_{i-1} & x_i \end{bmatrix} \left\{ \begin{array}{l} \partial \mathbf{x}_{\beta i} / \partial x \\ \partial \mathbf{x}_{\beta i} / \partial y \\ \partial \mathbf{x}_{\beta i} / \partial z \\ \partial^2 \mathbf{x}_{\beta i} / \partial x^2 \\ \partial^2 \mathbf{x}_{\beta i} / \partial y^2 \\ \partial^2 \mathbf{x}_{\beta i} / \partial z^2 \\ \partial^2 \mathbf{x}_{\beta i} / \partial x \partial y \\ \partial^2 \mathbf{x}_{\beta i} / \partial x \partial z \\ \partial^2 \mathbf{x}_{\beta i} / \partial y \partial z \end{array} \right. \quad (\text{B23})$$

Appendix C: Kriging Estimator

In normal Kriging the right hand term of the Kriging system (Eq. 4) corresponds to covariances and
 drift matrices of dimensions $m \times n$ where m is the number of elements of the data sets—either \mathbf{x}_α
 1300 or \mathbf{x}_β —and n the number of locations where the interpolation is performed, \mathbf{x}_0 .

Since, in this case, the parameters of the variogram functions are arbitrarily chosen, the Kriging variance does not hold any physical information of the domain. As a result of this, being interested only in the mean value, we can solve the Kriging system in the dual form (Matheron, 1981)(Chiles and Delfiner, 2009; Matheron, 1981)

$$1305 \quad Z(\mathbf{x}_0) = \begin{bmatrix} a'_{\partial \mathbf{Z}/\partial \mathbf{u}, \partial \mathbf{Z}/\partial \mathbf{v}} & b'_{\mathbf{Z}, \mathbf{Z}} & c' \end{bmatrix} \begin{bmatrix} \mathbf{c}_{\partial \mathbf{Z}/\partial \mathbf{u}, \partial \mathbf{Z}/\partial \mathbf{v}} & \mathbf{c}_{\partial \mathbf{Z}/\partial \mathbf{u}, \mathbf{Z}} \\ \mathbf{c}_{\mathbf{Z}, \partial \mathbf{Z}/\partial \mathbf{u}} & \mathbf{c}_{\mathbf{Z}, \mathbf{Z}} \\ \mathbf{f}_{10} & \mathbf{f}_{20} \end{bmatrix} \quad (\text{C1})$$

where:

$$\begin{bmatrix} a_{\partial \mathbf{Z}/\partial \mathbf{u}, \partial \mathbf{Z}/\partial \mathbf{v}} \\ b_{\mathbf{Z}, \mathbf{Z}} \\ c \end{bmatrix} = \begin{bmatrix} \partial \mathbf{Z} \\ 0 \\ 0 \end{bmatrix} \begin{bmatrix} \mathbf{C}_{\partial \mathbf{Z}/\partial \mathbf{u}, \partial \mathbf{Z}/\partial \mathbf{v}} & \mathbf{C}_{\partial \mathbf{Z}/\partial \mathbf{u}, \mathbf{Z}} & \mathbf{U}_{\partial \mathbf{Z}/\partial \mathbf{u}} \\ \mathbf{C}_{\mathbf{Z}, \partial \mathbf{Z}/\partial \mathbf{u}} & \mathbf{C}_{\mathbf{Z}, \mathbf{Z}} & \mathbf{U}_{\mathbf{Z}} \\ \mathbf{U}'_{\partial \mathbf{Z}/\partial \mathbf{u}} & \mathbf{U}'_{\mathbf{Z}} & \mathbf{0} \end{bmatrix}^{-1} \quad (\text{C2})$$

noticing that the 0 on the second row appears due to we are interpolation the difference of scalar fields instead the scalar field itself 2.

1310 **Appendix D: Example of covariance function: cubic**

The choice of the covariance function will govern the shape of the iso-surfaces of the scalar field. As opposed to other Kriging uses, here the choice cannot be based on empirical measurements. Therefore, the choice of the covariance function is merely arbitrary trying to mimic as far as possible coherent geological structures.

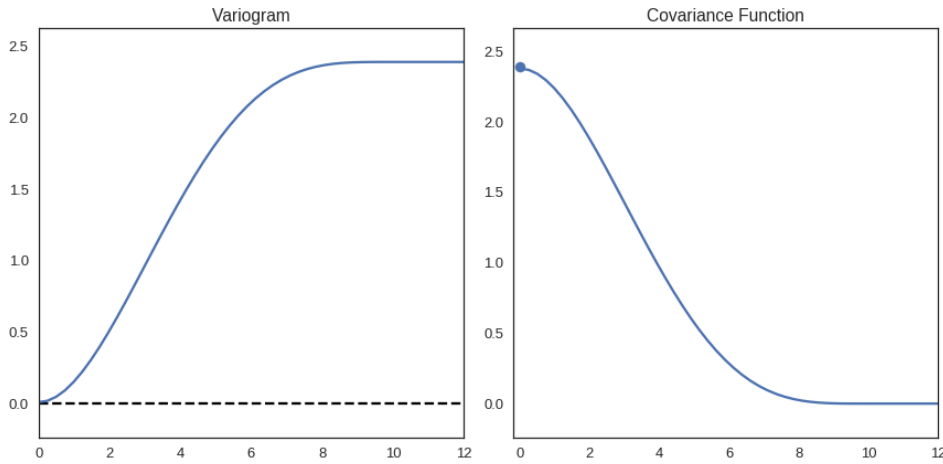


Figure 13. Representation of a cubic variogram and covariance for an arbitrary range and nugget effect.

1315 The main requirement to take into consideration when the time comes to choose a covariance function is that it has to be twice differentiable, h^2 in origin to be able to calculate $\mathbf{C}_{\partial \mathbf{Z}/\partial \mathbf{u}, \partial \mathbf{Z}/\partial \mathbf{v}}$ as

we saw in equation B13. The use of a Gaussian model $C(r) = \exp -(r/a)^2$ and the non-divergent spline $C(r) = r^4 \text{Log}(r)$ and their correspondent flaws are explored in Lajaunie et al. (1997).

The most widely used function in the potential field method is the cubic covariance due to mathematical robustness and its coherent geological description of the space.

$$C(r) = \begin{cases} C_0(1 - 7(\frac{r}{a})^2 + \frac{35}{4}(\frac{r}{a})^3 - \frac{7}{2}(\frac{r}{a})^5 + \frac{3}{4}(\frac{r}{a})^7) & \text{for } 0 \leq r \leq a \\ 0 & \text{for } r \geq a \end{cases} \quad (\text{D1})$$

with a being the range and C_0 the variance of the data. The value of a determine the maximum distance that a data point influence another. Since, we assume that all data belong to the same depositional phase it is recommended to choose values close to the maximum extent to interpolate in order to avoid mathematical artifacts. for the values of the covariance at 0 and nuggets effects so far only *ad hoc* values have been used so far. It is important to notice that the only effect that the values of the covariance in the potential-field method has it is to weight the relative influence of both CoKriging parameters (interfaces and orientations) since the absolute value of the field is meaningless. Regarding the nugget effect, the authors recommendation is to use fairly small nugget effects to give stability to the computation—since we normally use the kriging mean it should not have further impact to the result.

Appendix E: ~~Probabilistic Graphical Model~~ checking and diagnostics

~~Here we can see the probabilistic graphical model of the Bayesian inference of Section 3.4.2: Estimating convergence of Markov chain Monte Carlo simulations. We show here selected plots to evaluate convergence of the MCMC process. In figure 15, we present trace plots for selected parameters, and, in figure 14, the corresponding plots of the calculated Geweke statistics (Geweke et al., 1991). These parameters have been selected to show the overall range of convergence and trace behavior. Overall, the sampling algorithm performs well, although in some cases the step length could be adjusted further. Also, the Geweke statistics for some parameters fall partly outside of 2 standard deviations, indicating that the chain may not have fully converged. As described in the Discussion, we will attempt to address these issues with the use of a faster implementation of the modeling algorithm and by considering better sampling strategies in future work.~~

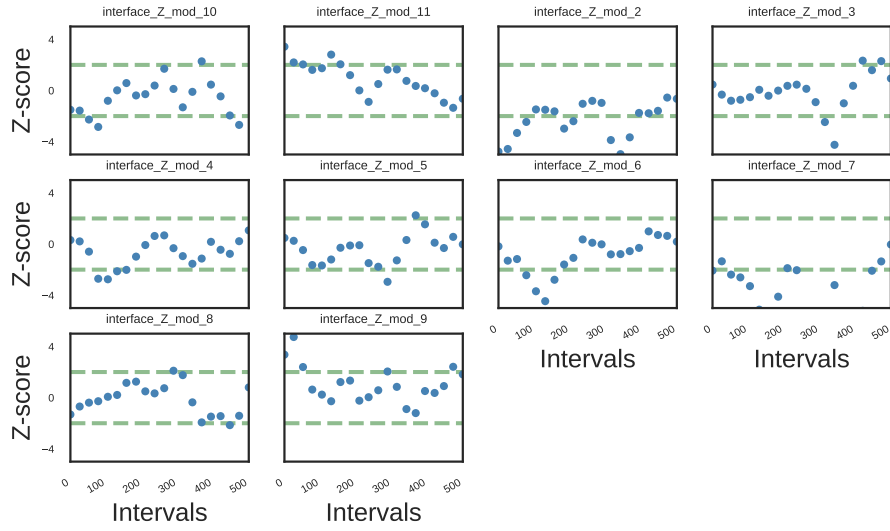


Figure 14. Probabilistic-graphical-model-generated-with-pymc2. Ellipses represent stochastic-Geweke values of the parameters, while triangles are deterministic functions that return intermediated states belonging to the inference of all likelihoods. Every point represents the probabilistic-model-such-as-mean of separated intervals of the GemPy-modelchain. If interval A and interval B belong to the same distribution, most of the Z-score should fall within 2 SD.

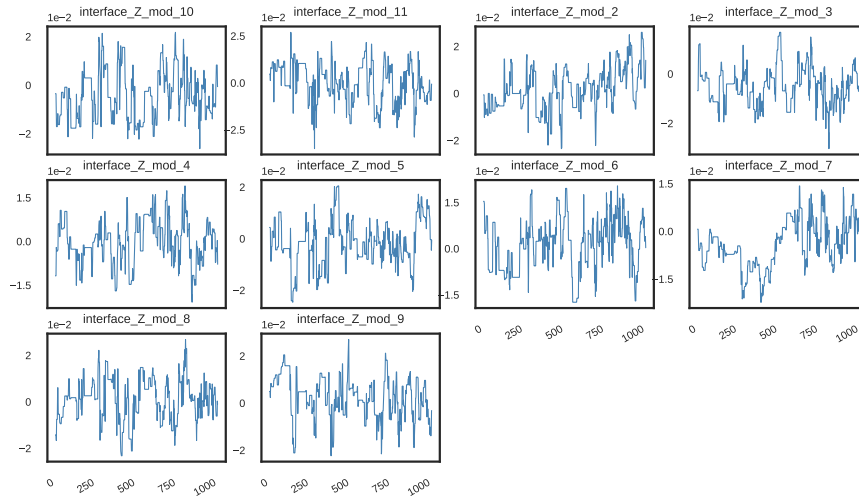


Figure 15. Traces of the parameters belonging to the inference with all likelihoods. The asymptotic behavior probes ergodicity. The first 1000 iterations (not displayed here) were used as burn-in and are not represented here.

Appendix F: Blender integration

Along the paper we have mentioned and show Blender visualizations (figure 1, b). The first step to
 1345 obtain them is to be able to run *GemPy* in Blender’s integrated Python (there are several tutorials
 online to use external libraries in Blender). Once it is running, we can use Blender’s library *bpy*
 to generate Blender’s actors directly from code. Here We include the code listing with the extra
 functions necessary to create automatically *GemPy* models in Blender

Listing 8. Extra functionality needed to create *GemPy* models in Blender

```

1350 # Import Blender library, GemPy and GemPy colors
import bpy
import gempy as gp
from gempy.colors import color_lot

1355 # Delete previous objects
try:
    bpy.ops.object.mode_set(mode='OBJECT')
    bpy.ops.object.select_by_type(type='MESH')
    bpy.ops.object.delete(use_global=False)
    for item in bpy.data.meshes:
        bpy.data.meshes.remove(item)
except:
    pass

```

```

1365 # Define functio to create a Blender material, i.e. texture
def makeMaterial(name, diffuse, specular, alpha):
    mat = bpy.data.materials.new(name)
    mat.diffuse_color = diffuse
1370 #mat.diffuse_shader = LAMBERT
    mat.diffuse_intensity = 1.0
    mat.specular_color = specular
    # mat.specular_shader = COOKTORR
    mat.specular_intensity = 0.5
1375 mat.alpha = alpha
    mat.ambient = 1
    return mat

# Define function the assing material to object
1380 def setMaterial(ob, mat):
    me = ob.data
    me.materials.append(mat)

...
1385 add listing 1
...

# Create interface spheres and orientation copes out of a (rescaled) geodata
# Interfaces
1390 for e, val in enumerate(interp_data.geo_data_res.interfaces.iterrows()):
    index = val[0]
    row = val[1]
    color = makeMaterial('color', color_lot[row['formation_number']], (1,1,1),1)
    origin = (row['X']*10, row['Y']*10, row['Z']*10)
1395 bpy.ops.mesh.primitive_uv_sphere_add(location=origin, size=0.1)
    setMaterial(bpy.context.object, color)

# Orientations
for e, val in enumerate(interp_data.geo_data_res.orientations.iterrows()):
1400 index = val[0]
    row = val[1]
    red = makeMaterial('Red', color_lot[row['formation_number']], (1,1,1),1)
    origin = (row['X']*10, row['Y']*10, row['Z']*10)
    rotation_p = (row['G_y'], row['G_x'], row['G_z'])
1405 bpy.ops.mesh.primitive_cone_add(location=origin, rotation=rotation_p)
    bpy.context.object.dimensions = [.3,.3,.3]
    #bpy.ops.transform.translate(value=(1,0,0))
    setMaterial(bpy.context.object, red)

1410 # Create rescaled simpleces
verts, faces = gp.get_surfaces(interp_data, lith_block[1],
                                fault_block[1],
                                original_scale=False)

# or import them from a previous project
1415 import numpy as np
verts = np.load('perth_ver.npy')
faces = np.load('perth_sim.npy')

# Create surfaces

```

```
1420 for i in range(0,n_formation):
    mesh_data = bpy.data.meshes.new("cube_mesh_data")
    mesh_data.from_pydata(verts[i]*10, [], faces[i].tolist())
    mesh_data.update()

1425     obj = bpy.data.objects.new("My_Object", mesh_data)
    red = makeMaterial('Red',color_lot[i+1],(1,1,1),1)
    setMaterial(obj, red)
    scene = bpy.context.scene
    scene.objects.link(obj)

1430     obj.select = True
```

Acknowledgements. The authors would like to acknowledge all people—all around the world—who has contributed to the final state of the library either by stimulating mathematical discussions or finding *bugs*. This project could not be possible without the invaluable help of all them.

1435 **References**

- Aug, C.: Modélisation géologique 3D et caractérisation des incertitudes par la méthode du champ de potentiel: PhD thesis, Ph.D. thesis, ENSMP, Paris, 2004.
- Ayachit, U.: The paraview guide: a parallel visualization application, 2015.
- Bardossy, G. and Fodor, J.: Evaluation of Uncertainties and Risks in Geology: New Mathematical Approaches
1440 for their Handling, Springer, Berlin, Germany, 2004.
- Baydin, A. G., Pearlmutter, B. A., Radul, A. A., and Siskind, J. M.: Automatic differentiation in machine learning: a survey, arXiv preprint arXiv:1502.05767, 2015.
- Bellman, R.: Dynamic programming, Courier Corporation, 2013.
- Betancourt, M., Byrne, S., Livingstone, S., Girolami, M., et al.: The geometric foundations of Hamiltonian
1445 Monte Carlo, *Bernoulli*, 23, 2257–2298, 2017.
- Bishop, C. M.: Model-based machine learning, *Phil. Trans. R. Soc. A*, 371, 20120222, 2013.
- Blender Online Community: Blender - a 3D modelling and rendering package, Blender Foundation, Blender Institute, Amsterdam, <http://www.blender.org>, 2017.
- Bond, C. E.: Uncertainty in structural interpretation: Lessons to be learnt, *Journal of Structural Geology*, 74,
1450 185–200, 2015.
- Bond, C. E., Gibbs, A. D., Shipton, Z. K., and Jones, S.: What do you think this is? “Conceptual uncertainty” in geoscience interpretation, *GSA Today*, 17, 4, 2007.
- Caers, J.: Introduction, in: *Modeling Uncertainty in the Earth Sciences*, pp. 1–8, John Wiley & Sons, Ltd, Chichester, UK, 2011.
- 1455 Calcagno, P., Chiles, J.-P., Courrioux, G., and Guillen, A.: Geological modelling from field data and geological knowledge: Part I. Modelling method coupling 3D potential-field interpolation and geological rules: Recent Advances in Computational Geodynamics: Theory, Numerics and Applications, *Physics of the Earth and Planetary Interiors*, 171, 147–157, 2008.
- Caumon, G.: Towards Stochastic Time-Varying Geological Modeling, *Mathematical Geosciences*, 42, 555–569,
1460 2010.
- Caumon, G., Collon-Drouaillet, P., Le Carlier de Veslud, C., Viseur, S., and Sausse, J.: Surface-Based 3D Modeling of Geological Structures, *Mathematical Geosciences*, 41, 927–945, 2009.
- Caumon, G., Gray, G., Antoine, C., and Titeux Marc-Olivier: Three-Dimensional Implicit Stratigraphic Model Building From Remote Sensing Data on Tetrahedral Meshes: Theory and Application to a Regional Model of
1465 La Popa Basin, NE Mexico, *IEEE Transactions on Geoscience and Remote Sensing*, 51, 1613–1621, 2013.
- Chatfield, C.: Model Uncertainty, Data Mining and Statistical Inference, *Journal of the Royal Statistical Society. Series A (Statistics in Society)*, 158, 419–466, 1995.
- Chiles, J.-P. and Delfiner, P.: *Geostatistics: modeling spatial uncertainty*, vol. 497, John Wiley & Sons, 2009.
- Chiles, J.-P., Aug, C., Guillen, A., and Lees, T.: Modelling of Geometry of Geological Units and its Uncertainty
1470 in 3D From Structural Data:~The Potential-Field Method, Perth, 2004.
- Christakos, G.: On the assimilation of uncertain physical knowledge bases: Bayesian and non-Bayesian techniques, *Advances in Water Resources*, 25, 1257–1274, 2002.

- Cockett, R., Kang, S., Heagy, L. J., Pidlisecky, A., and Oldenburg, D. W.: SimPEG: An open source framework for simulation and gradient based parameter estimation in geophysical applications, *Computers & Geosciences*, 85, 142–154, 2015.
- Cohen, J. S.: *Computer algebra and symbolic computation: Mathematical methods*, Universities Press, 2003.
- Dagum, L. and Menon, R.: OpenMP: an industry standard API for shared-memory programming, *IEEE computational science and engineering*, 5, 46–55, 1998.
- de la Varga, M. and Wellmann, J. F.: Structural geologic modeling as an inference problem: A Bayesian perspective, *Interpretation*, 4, 1–16, 2016.
- Dentith, M. and Mudge, S. T.: *Geophysics for the mineral exploration geoscientist*, Cambridge University Press, 2014.
- Duane, S., Kennedy, A. D., Pendleton, B. J., and Roweth, D.: Hybrid monte carlo, *Physics letters B*, 195, 216–222, 1987.
- Fiorio, C. and Gustedt, J.: Two linear time union-find strategies for image processing, *Theoretical Computer Science*, 154, 165–181, 1996.
- Geuzaine, C. and Remacle, J.-F.: Gmsh: A 3-D finite element mesh generator with built-in pre-and post-processing facilities, *International journal for numerical methods in engineering*, 79, 1309–1331, 2009.
- Geweke, J. et al.: Evaluating the accuracy of sampling-based approaches to the calculation of posterior moments, vol. 196, Federal Reserve Bank of Minneapolis, Research Department Minneapolis, MN, USA, 1991.
- Gonçalves, Í. G., Kumaira, S., and Guadagnin, F.: A machine learning approach to the potential-field method for implicit modeling of geological structures, *Computers & Geosciences*, 103, 173–182, 2017.
- Haario, H., Saksman, E., and Tamminen, J.: An adaptive metropolis algorithm. *Bernoulli* 7 223–242, *Mathematical Reviews (MathSciNet)*: MR1828504 Digital Object Identifier: doi, 10, 3318 737, 2001.
- Hillier, M. J., Schetselaar, E. M., de Kemp, E. A., and Perron, G.: Three-Dimensional Modelling of Geological Surfaces Using Generalized Interpolation with Radial Basis Functions, *Mathematical Geosciences*, 46, 931–953, 2014.
- Hoffman, M. D. and Gelman, A.: The No-U-turn sampler: adaptively setting path lengths in Hamiltonian Monte Carlo., *Journal of Machine Learning Research*, 15, 1593–1623, 2014.
- Hunter, J. D.: Matplotlib: A 2D graphics environment, *Computing In Science & Engineering*, 9, 90–95, 2007.
- Jaccard, P.: The distribution of the flora in the alpine zone., *New phytologist*, 11, 37–50, 1912.
- Jessell, M. W., Ailleres, L., and Kemp, A. E.: Towards an Integrated Inversion of Geoscientific data: what price of Geology?, *Tectonophysics*, 490, 294–306, 2010.
- Jordan, M. I.: *Learning in graphical models*, vol. 89, Springer Science & Business Media, 1998.
- Koller, D. and Friedman, N.: *Probabilistic graphical models: principles and techniques*, 2009.
- Kucukelbir, A., Ranganath, R., Gelman, A., and Blei, D.: Automatic variational inference in Stan, in: *Advances in neural information processing systems*, pp. 568–576, 2015.
- Kucukelbir, A., Tran, D., Ranganath, R., Gelman, A., and Blei, D. M.: Automatic differentiation variational inference, *arXiv preprint arXiv:1603.00788*, 2016.
- Lajaunie, C., Courrioux, G., and Manuel, L.: Foliation fields and 3D cartography in geology: Principles of a method based on potential interpolation, *Mathematical Geology*, 29, 571–584, 1997.

- Lark, R. M., Mathers, S. J., Thorpe, S., Arkley, S. L. B., Morgan, D. J., and Lawrence, D. J. D.: A statistical assessment of the uncertainty in a 3-D geological framework model, *Proceedings of the Geologists' Association*, 124, 946–958, 2013.
- 1515 Lauritzen, S. L., Dawid, A. P., Larsen, B. N., and Leimer, H.-G.: Independence properties of directed Markov fields, *Networks*, 20, 491–505, 1990.
- Lawson, C. L., Hanson, R. J., Kincaid, D. R., and Krogh, F. T.: Basic linear algebra subprograms for Fortran usage, *ACM Transactions on Mathematical Software (TOMS)*, 5, 308–323, 1979.
- Lindsay, M., Ailleres, L., Jessell, M. W., de Kemp, E., and Betts, P. G.: Locating and quantifying geological
1520 uncertainty in three-dimensional models: Analysis of the Gippsland Basin, southeastern Australia, *Tectonophysics*, 546–547, 10–27, 2012.
- Lindsay, M. D., Jessell, M. W., Ailleres, L., Perrouy, S., de Kemp, E., and Betts, P. G.: Geodiversity: Exploration of 3D geological model space, *Tectonophysics*, 594, 27–37, 2013a.
- Lindsay, M. D., Perrouy, S., Jessell, M. W., and Ailleres, L.: Making the link between geological and geophysical uncertainty: geodiversity in the Ashanti Greenstone Belt, *Geophysical Journal International*, 195,
1525 903–922, 2013b.
- Lorensen, W. E. and Cline, H. E.: Marching cubes: A high resolution 3D surface construction algorithm, in: *ACM siggraph computer graphics*, vol. 21, pp. 163–169, ACM, 1987.
- Mallet, J.-L.: Space-time mathematical framework for sedimentary geology, *Mathematical Geology*, 36, 1–32,
1530 2004.
- Marechal, A.: Kriging seismic data in presence of faults, in: *Geostatistics for natural resources characterization*, pp. 271–294, Springer, 1984.
- Matheron, G.: Splines and kriging: their formal equivalence, *Down-to-earth-statistics: Solutions looking for geological problems*, pp. 77–95, 1981.
- 1535 McKinney, W.: pandas: a foundational Python library for data analysis and statistics, *Python for High Performance and Scientific Computing*, pp. 1–9, 2011.
- McLane, M., Gouveia, J., Citron, G. P., MacKay, J., and Rose, P. R.: Responsible reporting of uncertain petroleum reserves, *AAPG Bulletin*, 92, 1431–1452, 2008.
- Mosegaard, K. and Tarantola, A.: Monte Carlo sampling of solutions to inverse problems, *Journal of Geophysical Research*, 100, 12–431, 1995.
1540
- Nabighian, M. et al.: 75 anniversary-The historical development of the gravity method in exploration, *Geophysics*, 70, 2005.
- Nagy, D.: The gravitational attraction of a right rectangular prism, *Geophysics*, 31, 362–371, 1966.
- Normark, K.: Overview of the four main programming paradigms, 2013.
- 1545 Ogilvie, J. F.: A Monte-Carlo approach to error propagation, *Computers & chemistry*, 8, 205–207, 1984.
- Patil, A., Huard, D., and Fonnesbeck, C. J.: PyMC: Bayesian stochastic modelling in Python, *J. Stat. Softw.*, pp. 1–81, 2010.
- Rall, L. B.: Automatic differentiation: Techniques and applications, 1981.
- Robitaille, T. P., Tollerud, E. J., Greenfield, P., Droettboom, M., Bray, E., Aldcroft, T., Davis, M., Ginsburg,
1550 A., Price-Whelan, A. M., Kerzendorf, W. E., et al.: Astropy: A community Python package for astronomy, *Astronomy & Astrophysics*, 558, A33, 2013.

- Salvatier, J., Wiecki, T. V., and Fonnesbeck, C.: Probabilistic programming in Python using PyMC3, *PeerJ Computer Science*, 2, e55, 2016.
- Sambridge, M. and Mosegaard, K.: Monte Carlo methods in geophysical inverse problems, *Rev. Geophys.*, 40, 1555–2002, 2002.
- Schaaf, A.: Geological Inference based on Kinematic Structural Models, Master's thesis, RWTH Aachen University, Aachen, Germany, 2017.
- Schroeder, W. J., Lorensen, B., and Martin, K.: The visualization toolkit: an object-oriented approach to 3D graphics, Kitware, 2004.
- 1560 Shannon, E. C.: A mathematical theory of communication, *Bell System Technical Journal*, 27, 1948.
- Stamm, F. A.: Bayesian Decision Theory in Structural Geological Modeling - How Reducing Uncertainties Affects Reservoir Value Estimations, Master's thesis, RWTH Aachen University, Aachen, Germany, 2017.
- Tarantola, A.: Inverse problem theory and methods for model parameter estimation, *Society for Industrial Mathematics*, 2005.
- 1565 Tarantola, A. and Valette, B.: Inverse Problems = Quest for Information, *Journal of Geophysics*, 50, 159–170, 1982.
- Theano Development Team: Theano: A Python framework for fast computation of mathematical expressions, *arXiv e-prints*, abs/1605.02688, <http://arxiv.org/abs/1605.02688>, 2016.
- Thiele, S. T., Jessell, M. W., Lindsay, M., Ogarko, V., Wellmann, J. F., and Pakyuz-Charrier, E.: The topology of geology 1: Topological analysis, *Journal of Structural Geology*, 91 IS -, 27–38, 2016a.
- 1570 Thiele, S. T., Jessell, M. W., Lindsay, M., Wellmann, J. F., and Pakyuz-Charrier, E.: The topology of geology 2: Topological uncertainty, *Journal of Structural Geology*, 91, 74–87, 2016b.
- Van der Walt, S., Schönberger, J. L., Nunez-Iglesias, J., Boulogne, F., Warner, J. D., Yager, N., Gouillart, E., and Yu, T.: scikit-image: image processing in Python, *PeerJ*, 2, e453, 2014.
- 1575 van der Walt, S., Schönberger, J. L., Nunez-Iglesias, J., Boulogne, F., Warner, J. D., Yager, N., Gouillart, E., Yu, T., and the scikit-image contributors: scikit-image: image processing in Python, *PeerJ*, 2, e453, doi:10.7717/peerj.453, <http://dx.doi.org/10.7717/peerj.453>, 2014.
- van Rossum, G., Warsaw, B., and Coghlan, N.: PEP 8: style guide for Python code, *Python. org*, 2001.
- Wackernagel, H.: Multivariate geostatistics: an introduction with applications, *Springer Science & Business Media*, 2013.
- 1580 Walt, S. v. d., Colbert, S. C., and Varoquaux, G.: The NumPy array: a structure for efficient numerical computation, *Computing in Science & Engineering*, 13, 22–30, 2011.
- Wang, H., Wellmann, J. F., Li, Z., Wang, X., and Liang, R. Y.: A Segmentation Approach for Stochastic Geological Modeling Using Hidden Markov Random Fields, *Mathematical Geosciences*, 49, 145–177, 2017.
- 1585 Waskom, M., Botvinnik, O., O’Kane, D., Hobson, P., Lukauskas, S., Gemperline, D. C., Augspurger, T., Halchenko, Y., Cole, J. B., Warmenhoven, J., de Ruiter, J., Pye, C., Hoyer, S., Vanderplas, J., Villalba, S., Kunter, G., Quintero, E., Bachant, P., Martin, M., Meyer, K., Miles, A., Ram, Y., Yarkoni, T., Williams, M. L., Evans, C., Fitzgerald, C., Brian, Fonnesbeck, C., Lee, A., and Qalieh, A.: mwaskom/seaborn: v0.8.1 (September 2017), doi:10.5281/zenodo.883859, <https://doi.org/10.5281/zenodo.883859>, 2017.
- 1590 Wellmann, J. F. and Regenauer-Lieb, K.: Uncertainties have a meaning: Information entropy as a quality measure for 3-D geological models, *Tectonophysics*, 526–529, 207–216, 2012.

- Wellmann, J. F., Horowitz, F. G., Schill, E., and Regenauer-Lieb, K.: Towards incorporating uncertainty of structural data in 3D geological inversion, *Tectonophysics*, 490, 141–151, 2010.
- Wellmann, J. F., Lindsay, M., Poh, J., and Jessell, M. W.: Validating 3-D Structural Models with Geological
1595 Knowledge for Improved Uncertainty Evaluations, *Energy Procedia*, 59, 374–381, 2014.
- Wellmann, J. F., Thiele, S. T., Lindsay, M. D., and Jessell, M. W.: pynoddy 1.0: an experimental platform for automated 3-D kinematic and potential field modelling, *GMD*, 9, 1019–1035, 2016.
- Wellmann, J. F., de la Varga, M., Murdie, R. E., Gessner, K., and Jessell, M.: Uncertainty estimation for a geological model of the Sandstone greenstone belt, Western Australia—insights from integrated geological and
1600 geophysical inversion in a Bayesian inference framework, *Geological Society, London, Special Publications*, 453, SP453–12, 2017.
- Wu, K., Otoo, E., and Shoshani, A.: Optimizing connected component labeling algorithms, Lawrence Berkeley National Laboratory, 2005.